Eur. Phys. J. Spec. Top.
https://doi.org/10.1140/epjs/s11734-024-01189-0

THE EUROPEAN PHYSICAL JOURNAL SPECIAL TOPICS

Review

X-ray scatterings to probe the structure and assembly of biomimetic membranes

Ajit Seth[a], Devansh Kaushik[b], and Sajal K. Ghosh[c]

Department of Physics, Shiv Nadar Institution of Eminence, NH-91, Tehsil Dadri, Gautam Buddha Nagar, Uttar Pradesh 201314, India

Received 15 February 2024 / Accepted 23 May 2024

Abstract Biomimetic membranes are the model membranes formed with a few chemical components, particularly with phospholipids that closely follow a biological membrane. There are multiple experimental techniques to probe the physio-chemical properties and structure of such systems. X-ray scattering techniques are the important ones as they are non-destructive in nature and can provide structural details about the assembly of molecules in the membrane at sub-nanometer length scale. In this review, major techniques, such as small angle X-ray scattering (SAXS), X-ray reflectivity (XRR), and grazing incidence X-ray diffraction (GIXD) have been discussed with a focus on the structural aspect of membranes. One of these techniques is chosen depending upon the model membranes that include the lipid monolayer at air–water interface, unilamellar vesicles (ULV), multilamellar vesicles (MLV), single- or multi-layer of membranes on a solid or a soft support. A few recent results have also been discussed that are obtained by utilizing the advanced synchrotron-based X-ray scattering techniques. Finally, a few challenges and future aspects in the research field have been presented.

1 Introduction

The viability of a cell and its inner organelles depends on the existence of a biological membrane. The selective permeability provided by this membrane, towards ions and molecules, allows it to maintain a concentration gradient across the cell [1]. These biological membranes are a mixture of lipids, proteins and many other molecules [2–5]. Each of these components influences the mechanical, structural, physical, and chemical changes that occur in the membrane, or that are mediated by it [5–7]. The structure of this membrane is composed of a double leaflet of lipids known as the lipid bilayer, with proteins and other macromolecules embedded into the leaflets. These lipids can either be phospholipids or glycolipids and are amphiphilic in nature with a hydrophilic water-loving head group and one or two hydrophobic water repelling hydrocarbon chains [8].

The study of biological membranes requires suitable consideration of their complexity, thereby posing a great challenge to experimental and theoretical approaches [9, 10]. Ideally, in order to extract molecular level information about the chemistry of real biological membranes, the probing methods should be label-free, non-perturbing and interface specific. Further, the methods should be able to discern different chemical structures with high spatial and temporal resolution on multiple length scales, and capable of measuring in a media. As chemistry of living systems involves a complex and delicate balance of hundreds of components, no in vivo technological advancements have been made to provide in-depth and exact analysis about the actual biological cell membrane [11]. Through optics and microscopy, one can access certain aspects of cellular functioning using dye molecules or nanoparticles, but no comprehensive and error free conclusions can be drawn [12–14]. In most of the cases, only probabilistic conclusions are drawn. Hence, researchers have been using simplified model systems that mimic certain aspects of membranes to effectively study the behavior of multiple additives in and around a membrane. These biomimetic

Ajit Seth and Devansh Kaushik have contributed equally to this work.

[a] e-mail: as984@snu.edu.in
[b] e-mail: dk912@snu.edu.in
[c] e-mail: sajal.ghosh@snu.edu.in (corresponding author)

Published online: 04 June 2024

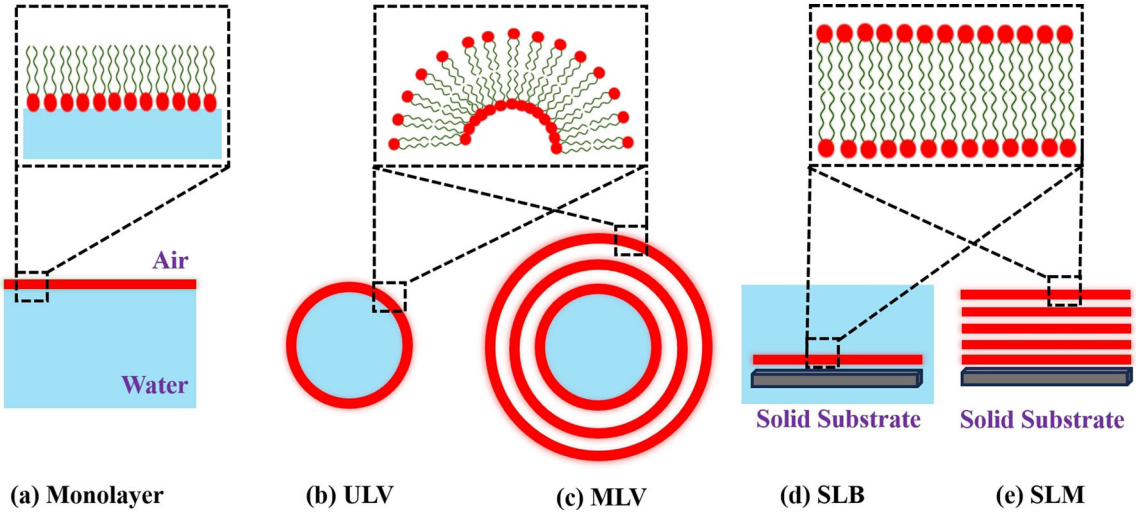

Fig. 1 Biomimetic lipid membranes in the form of **a** Monolayer, **b** Unilamellar vesicle (ULV), **c** Multilamellar Vesicle (MLV), **d** Supported lipid bilayer (SLB), and **e** Supported Lipid Multilayer (SLM)

model membrane systems can range from small scale arrangements like lipid monolayer and supported lipid bilayer (SLB), to larger and more realistic unilamellar vesicle (ULV) and multilamellar vesicle (MLV) (Fig. 1). Also, lipid bilayers can be stacked periodically on a solid substrate to form supported lipid multilayer (SLM). While a lipid monolayer is a one-molecule thick film of lipid molecules usually formed at the air-aqueous interface, the SLB is the deposited lipid-bilayer on a solid substrate either through vesicle fusion or the Langmuir Blodgett -Schaefer technique [15]. A vesicle is a self-assembled circular structure consisting of liquids enclosed by lipid bilayer. A ULV has a single lipid bilayer, while a MLV resembles layers of an onion with multiple bilayers. Each bilayer has opposing polar head group regions filling the intermediate volume with long hydrocarbon chains as shown in Fig. 1 [16]. The asymmetric distribution of lipids and proteins across the bilayer in the inner and outer leaflets plays a unique structural and biochemical role in cellular bio-mimicking [17]. The physical properties of vesicles, including their size, shape, and thermodynamic state are associated with their potential applications [18–21].

The chemical complexities involved in model membrane systems can be explored by coupling them with interface sensitive spectroscopic, scattering and analytical techniques. Optical microscopy can study membrane in situ under biologically relevant or other interesting conditions but with a limited spatial resolution [22]. The scanning probes such as scanning tunnelling, atomic force and scanning electron microscopy can provide information with higher spatial resolution, but they have limitations with sample environments that do not follow physiological conditions. Contrarily, techniques like X-ray and neutron scatterings provide quantitative data on the distribution of structural features, such as sizes, shapes and correlation lengths by providing a control for in situ manipulation of samples [23–25]. All the scattering techniques describe the constructive interference of waves scattered, or reflected, from atoms at different angles from the direction of the incoming wave, be it electromagnetic waves of X-rays or the quantum wave properties of a particle, such as a neutron or electron.

Generally, model lipid membranes exist in aqueous environment, hence the use of X-rays scattering becomes optimum for their studies as it allows for minimum intervention. In solution measurements, the systems can mimic physiological condition [27, 28]. Also, the high penetration capabilities of X-rays enable an experimental setup which is capable of taking measurements even at the nanoscale for macroscopic samples [29]. Furthermore, utilizing X-ray scattering for liquid crystalline lipid-based systems enhances the study of the Bragg diffraction of lipid mesophases and associated bio-molecules interacting with them [30–32]. Additionally, X-ray scattering-based measurements prove beneficial in resolving the wide range of layer length-scales found in lipid systems. For example, the hydrocarbon tail ordering being in the nanometre scale while the bilayer separation is typically few to tenths of nanometers [33]. Hence, X-ray scattering is a crucial technique to discover the lipid assembly in a membrane, the membrane elasticity and adsorption of foreign molecules to the membrane at various conditions [34, 35]. In this review, various X-ray scattering techniques and their uses in probing the structural details of different bio-mimetic membranes have been discussed. Figure 2 represents the schematic displaying the experimental set up for small angle X-ray scattering (SAXS), X-ray reflectivity (XRR) and grazing incidence X-ray diffraction (GIXD) [26, 36].

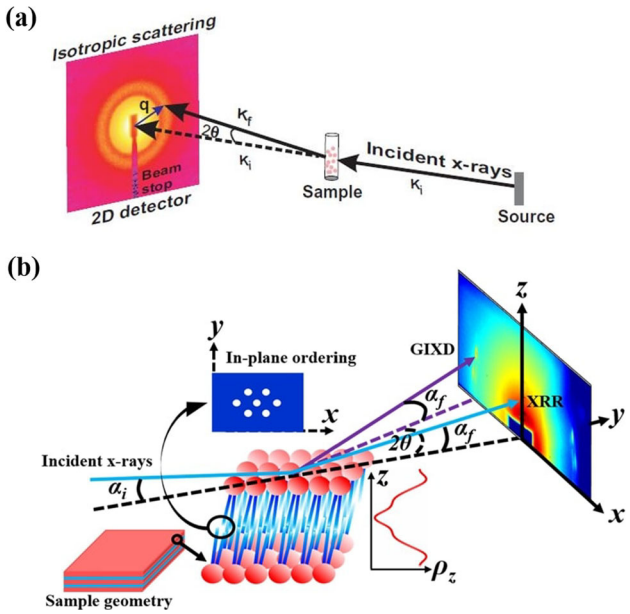

Fig. 2 Schematic illustration of the experimental set up for **a** Small Angle X-ray Scattering (SAXsS) and **b** X-Ray Reflectivity (XRR) and Grazing Incidence X-ray Diffraction (GIXD). **a** has been adapted with permission from Ref. [26]. Copyright © Deutsche Physikalische Gesellschaft. Reproduced by permission of IOP Publishing. CC BY-NC-SA. **b** has been adapted with permission from Elsevier, Ref. [36]

2 Small angle X-ray scattering (SAXS)

The diagram in Fig. 2a illustrates the setup for the SAXS experiment. In this experiment, generally, the solution of nano-structures are taken in a glass or quartz capillary and placed between the X-ray source and the detector. A focused beam passes through the sample in transmission mode, after which, the scattered photons are collected on a two-dimensional (2D) detector. Then the radially summed intensity is plotted against the wave vector [26]. The final data are achieved after suitable background subtraction.

SAXS provides information on the electron density profile of a lipid bilayer with a detailed picture of its structure [37]. With this technique, the precise positioning of any foreign molecule, such as a protein or drug, in a membrane can be resolved [10]. Further, the average number of bilayers present in an MLV along with the physical properties of a bilayer can be assessed [38].

2.1 Unilamellar vesicles (ULVs)

A ULV is recognized as a fundamental structure in the field of membrane biophysics, consisting of an aqueous core encapsulated in a single lipid bilayer (Fig. 1b). Based on size, ULVs can be categorized as small unilamellar vesicles (SUVs, 10–100 nm), large unilamellar vesicles (LUVs, 100–1000 nm) and giant unilamellar vesicles (GUVs, >1 μm) [39].Out of these, generally, SUVs and LUVs are suitable for the SAXS experiments. It has emerged as an instrument in the domain of nanotechnology and drug delivery. This vesicular structure provides a simpler model for studying membrane dynamics, interactions, and permeability properties of cellular interfaces [40]. The fundamentals of a ULV can be traced back to 1965 when Bangham et al. utilized ULVs to mimic biological membranes, for understanding the diffusion of univalent cations and anions across the phospholipid bilayer [41]. The structural and functional resemblance of ULVs to cell membranes has made them essential in studies ranging from lipid-protein interactions to the encapsulation and delivery of therapeutic agents [42, 43].

As mentioned above, the scattering signature observed on the 2D detector from the ULVs are radially integrated, providing an '*I-q plot*'; i.e., the X-ray scattering intensity, *I(q)* vs. wave vector, $q = 4\pi sin\theta/\lambda$ plot, where 2θ is the scattering angle (Fig. 2a). For vesicles, the scattering intensity is given by [44]

$$I(q) \propto P(q)S(q) \tag{1}$$

where $P(q)$ is the particle structure factor, and $S(q)$ is the inter-particle structure factor. This $P(q)$ is equal to the square of the form factor *F(q)*, that is, the Fourier transform of the electron density ρ(r) of the bilayer [45]. The *F(q)* is expressed as,

$$F(q) = \int (\rho(r) - \rho(0)) \exp(-iq.r)\, dV \tag{2}$$

where $\rho(0)$ is the electron density of the buffer. In a dilute and weakly interacting system, the structure factor $S(q) = 1$ [46]. Hence, the Eq. 1 becomes [44],

$$\langle I(q) \rangle \propto \langle F(q)^2 \rangle \tag{3}$$

The electron density profile across the depth of a lipid bilayer can be viewed as a summation of n Gaussian, each representing a particular bilayer region. The model accounts for the amplitude ρ_k, average position δ_k, and positional uncertainty σ_k of each region k [46].

$$\rho(r) = \sum_{k=1}^{n} \rho_k \exp\left[-\frac{(r-\delta_k)^2}{(2\sigma_k^2)}\right]. \tag{4}$$

Here, δ_k is the distance from the center of the vesicle to the bilayer surface, which can be expressed as $\delta_k = R + \varepsilon_k$, where R is the radius of the vesicle and ε_k incorporates the displacement fluctuations. The center of the vesicle is taken to be at $r = 0$. In the case of a solution, the sample is a powder one with the vesicles in a completely random orientation. Then the form factor is given by,

$$F_f(q) = q^{-1} \sum_{k=1}^{n} \rho_k \sigma_k \exp\left(\frac{-q^2\sigma_k^2}{2}\right) \exp(\iota q \delta_k). \tag{5}$$

For a spherical, radially symmetric vesicle with n Gaussian shells, the intensity is given by [46],

$$I(q) = < F_f(q)^2 > = q^{-2} \sum_{k,\,k'}^{n} \rho_k \rho_{k'} \sigma_k \sigma_{k'} \exp\left[\frac{-q^2\left(\sigma_k^2 + \sigma_{k'}^2\right)}{2}\right] \cos\left[q(\varepsilon_k - \varepsilon_{k'})\right]. \tag{6}$$

The typical scattering profiles from the solutions of various micro-structures are depicted in Fig. 3a [47]. The profile from the ULV solution can be fitted with the theoretical expression of $I(q)$ discussed here to obtain the structural parameters of a ULV.

Recent advances have been made in the investigation of amphiphilic self-assembly processes, in particular of ULVs, using time-resolved SAXS in conjunction with rapid stopped-flow mixing. The study clarified the dynamic structural changes of the self-assembly of molecules into a vesicle, providing information about the millisecond timescale [49]. In 2011, Jeremie et al. probed the structural dynamics underlying the formation of a ULV upon mixing dilute solutions of anionic surfactant lithium perfluorooctanoate (LPFO) and zwitterionic surfactant tetradecyldimethylamine oxide (TDMAO) using time-resolved SAXS [47]. They quantified the concentration-dependent pathways in this spontaneous self-assembly of the surfactants. Figure 3a shows the time-resolved SAXS intensities after mixing solutions of TDMAO and LPFO. The first curve at 2.3 ms describes the disk-like structure with a mean radius of 6.0 nm and thickness of 4.0 nm. These disk-like micelles grow up to 200 ms to reach a radius of 10.0 nm and then they close to form a ULV. This process of formation of ULVs from disk-like structures lasts for 3 s, and the final ULV has a mean radius of 12.5 nm with a bilayer thickness of 3.6 nm. In 2014, Narayanan et al. put forth a study to advance the knowledge about the fundamental principles governing the self-assembly of ULVs, and their potential use in fields like targeted drug delivery [50]. They showed that the ULVs can be formed via many kinetic pathways, each of which leads to the final vesicle structure. The intermediates can involve disk-like or torus-like structures, depending on the initial concentration of surfactant in solutions. This study also highlights the importance of taking radiation damage into account and highlights the potential of SAXS to reveal multi-scale static and transient structures.

In 2021, a study by Chappa et al. contributed to understanding the asymmetry in vesicles with equal lipid distribution in small ULVs with high curvature [48]. By using SAXS, they quantified the impact of curvature on electron-density profiles of the ULVs. They simulated the scattering profiles including the polydispersity and thermal fluctuations. Their study, based on using direct modeling and the 3D Fourier Transform on a numerical grid, opened a door to the study of vesicular systems with embedded proteins. They used two different lipids, dioleoylphosphatidylcholine (DOPC) and dioleoylphosphatidylethanolamine (DOPE) in a (1:1) mixture, to form the ULVs using an extrusion method. The formed ULVs were immersed in glucose solution, to induce the osmotic pressure and vesicle deformation. Figure 3b shows the asymmetry in ULVs in the mixed lipid system in water, while Fig. 3c represents the induced asymmetry (shape transition) in ULVs in the presence of glucose, due to osmotic pressure. The results indicate a transition to a prolate shape, due to a decrease in water permeation by osmotic gradient.

Komorowski et al. showed the effect of divalent, Ca^{2+}, and Mg^{2+} ions on the ULVs [51]. The bilayer structure and inter-bilayer distance in the docking state were analyzed by SAXS. The presence of these ions leads to the

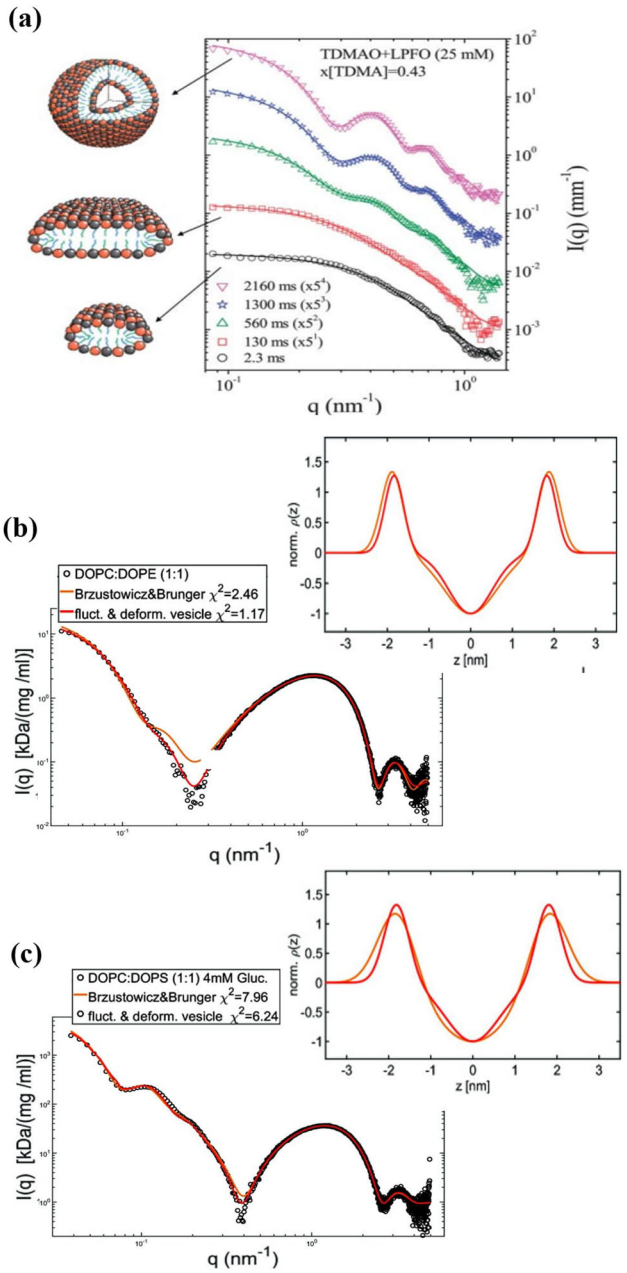

Fig. 3 **a** Small angle X-ray scattering profiles for the dynamic structural changes in the pathway of self-assembly from micelle (bottom profile) to ULV (top profile) in a mixed surfactant system. Reproduced from Ref. [47] with permission from the Royal Society of Chemistry. The scattering profiles from ULV in the presence and absence of glucose quantify the asymmetry in the mixed lipid system shown in **b** DOPC: DOPE, and **c** DOPC: DOPS.Adapted with permission from Ref. [48]

transition of pure dioleoylphosphatidylserine (DOPS) ULVs to MLVs, which is evident from the emerging Bragg peaks in Fig. 4a. The presence of divalent ions also increases the bilayer thickness. They also quantified the vesicle adhesion in a mixed vesicle (DOPC: DOPS, 1:1) system, in the presence of glucose and Ca^{2+}. Figure 4b shows the change in scattering profile arising due to adhesion between two different vesicles. The thickness of the water layer remains unchanged with a change in the concentration of the ions. This suggests the recruitment of Ca^{2+} to the contact zone is required to compensate for the charge of anionic membranes.

Even though there are numerous examples of ULVs prepared using synthetic lipids, very few SAXS investigations are reported on real biological vesicles. Castorph et al. have reported work on synaptic vesicles (SVs) which contain neurotransmitters [52]. These are the vesicles found in the synaptic terminal of neurons that play a pivotal role in neuronal communication. Using a synchrotron source, SAXS analysis provided a quantitative structural description of the vesicle with a detailed distribution of proteins in it. A critical analysis of the data indicated the existence of protein microdomains in the vesicle which was otherwise difficult to probe.

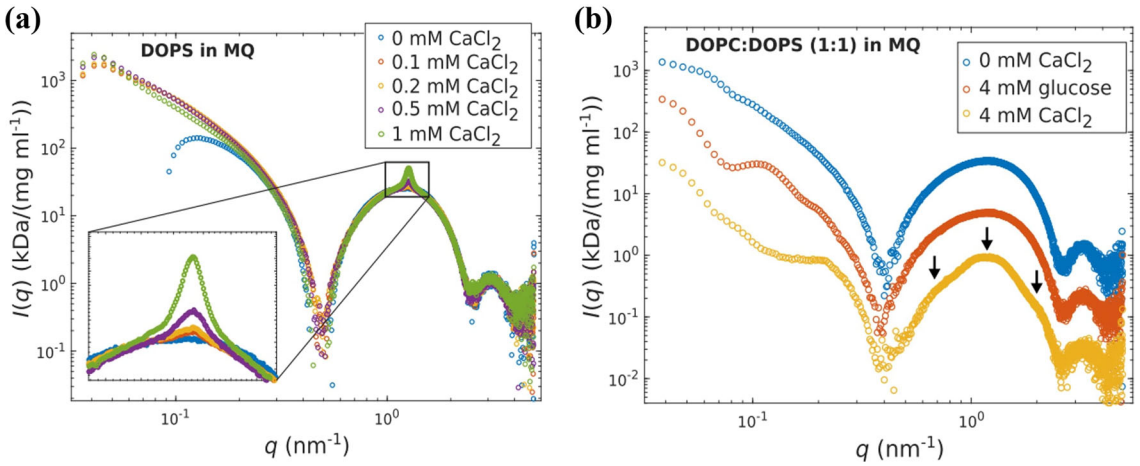

Fig. 4 **a** The emergence of Bragg peaks with the addition of divalent ions (Ca^{2+}), corresponding to the transition from ULV to MLV. **b** The vesicle adhesion in a mixed lipid system is due to the charge compensation of anionic lipids from divalent ions. Adapted with permission from Ref. [51]

2.2 Multilamellar vesicles (MLVs)

As introduced earlier, MLVs are characterized by concentric lipid bilayers, separated by aqueous compartments. These MLVs are beneficial for delivery applications for a higher volume of hydrophobic drugs as their mechanical properties are beneficial for cellular uptake. Studies have shown that they can be used to model the behavior of skin lipids, making them valuable in dermatological research [53]. Techniques such as SAXS have provided insights into the arrangement and spacing of the lipid bilayers within a MLV [54]. These studies have been instrumental in understanding the stability and permeability of MLVs, which are key factors in their functionality as molecule carriers along with other applications.

The method to obtain the transbilayer electron density profile from ULVs differs from those of MLVs. The ULVs consist of a single bilayer, and they are dispersed in the dilute aqueous solution without any inter-vesicle interactions. In such a case, the structure factor, $S(q)$ is taken to be unity ($S(q) = 1$). Here, the scattering profile is fitted by considering the form factor of the vesicle to obtain the transbilayer electron density profile. In the case of MLVs, the onion-like structure induces a lamellar phase, where a functional form of the structure factor must be considered as there is a correlation among the stacked bilayers. This makes the extraction of transbilayer electron density profile more complex [38]. In multilamellar vesicles, the form factor, $\mathcal{F}(q)$, is derived from the Fourier transform of electron density as it is done for a ULV. In addition, as each bilayer is stacked on each other forming a structure similar to a smectic liquid crystal, a structure factor is necessary for simulating the intensity profile. The paracrystalline theory [55] and Caille theory [56] are the popular ones for modeling the lattice structure factor for such a structure. The former describes the stochastic fluctuations of ideally flat layers, while the latter considers bilayer undulations. The modified Caille theory (MCT) [57], is adapted for smectic liquid crystals and accounts for the finite size of the lamellar stack. The expression for the structure factor is given by,

$$S(q) = N + 2 \sum_{k=1}^{N-1} (N-k)\cos(kqd)\; e^{-\left(\frac{d}{2\,\pi}\right)^2 q^2 \eta_1 \gamma} (\pi k)^{-\left(\frac{d}{2\,\pi}\right)^2 q^2 \eta_1}, \tag{7}$$

where N is the mean number of coherent scattering bilayers, γ is the Eulers' constant, and η_1 is the Callie parameter. The undulations [58] related to the bending modulus, K, and the bulk modulus, B of a membrane are combined in the Callie parameter [56], defined as,

$$\eta_h = \frac{q^2\; kT}{8\;\pi\sqrt{KB}} = \eta_1 h^2, \tag{8}$$

where k is the Boltzmann constant, T is temperature, and h is the order of reflection. The d is the repetitive distance between the bilayers including the thickness of a bilayer and the water layer between two successive

bilayers. The form factor is given by,

$$F(q) = \int \rho(z) \exp(\iota q z)\, \mathrm{d}z, \tag{9}$$

where $\rho(z)$ is the electron density along $\hat{z}$. This $\rho(z)$ of a bilayer is resolved by the summation of three Gaussians; two representing the polar heads of opposing monolayers and the third one describing the hydrocarbon chain region [59],

$$\rho(z) = \rho_w + \overline{\rho_H}\left[\exp\left(-\frac{(z-z_H)^2}{2\sigma_H^2}\right) + \exp\left(-\frac{(z+z_H)^2}{2\sigma_H^2}\right)\right] + \overline{\rho_C}\exp\left(-\frac{z^2}{2\sigma_C^2}\right). \tag{10}$$

Here, the electron densities of the head group ($\overline{\rho_H}$) and hydrocarbon tail ($\overline{\rho_C}$) are defined relative to the electron density of water, $\rho_w (= 0.334\ e/\text{Å}^3)$. These relative electron densities are represented as $\overline{\rho_H}$ $(= \rho_H - \rho_w)$, and $\overline{\rho_C}$ $(= \rho_C - \rho_w)$, where ρ_H and ρ_C are the actual electron densities of the head and tail, respectively. The Gaussian peak related to the lipid head is positioned at z_H, while the centre of the hydrocarbon tail is at z_C $(= 0)$, with the broadness of Gaussian distribution as, σ_H and σ_C, respectively. Using this model for electron density, the time-averaged form factor is defined as,

$$\begin{aligned}\langle F(q)\rangle &= 2F_H(q) + F_C(q)\\ &= \sqrt{2\,\pi}\left[\sigma_H\ \overline{\rho_H}\ \exp\left(-\frac{\sigma_H^2\ q^2}{2}\right)\cos(q\ z_H) + \ \sigma_C\ \overline{\rho_C}\ \exp\left(-\frac{\sigma_C^2\ q^2}{2}\right)\right]\end{aligned} \tag{11}$$

Considering the MCT and Gaussian electron density, Pabst et al. [60] obtained the complete scattering profile for an MLV system. Including the diffused scattering along with the Bragg peaks, the total scattering intensity is given by,

$$I(q) \propto \left(|F(q)|^2 S(q) + N_{\text{diff}}|F(q)|^2\right)\frac{1}{q^2}, \tag{12}$$

The term N_{diff} captures the essence of diffused scattering from positionally uncorrelated bilayers, and $\frac{1}{q^2}$ is the Lorentz correction factor. The complete q-range fit of the experimental data, using the above equation, provides the structural parameters, such as area per lipid, hydrocarbon chain length (d_C), bilayer thickness (d_B), the thickness of water layer (d_W) between two bilayers, the number of inter-bilayer free water per lipid molecule (n_W^*), and, the total number of water molecules intercalated into the bilayer (n_w). This was the first study to quantify the structural parameters without volumetric measurements, and directly from electron density profile [60].

Vancylenberg et al. have used MCT for fitting SAXS profiles from MLVs to find out minute details of water molecules in proximity to a lipid bilayers [61]. They categorized the water layer into three regions, (i) head-group water, (ii) perturbed water, and (iii) free water (see Fig. 5b). The blue curve in Fig. 5a, depicts the scattering from MLVs of DMPC with the fit shown in the red line. The thickness of different sub-layers of interstitial water was calculated at different temperatures (see Figs. 5c and 6). The difference between the two lipids, DMPC and DMPE can be seen through the behavior of d_w which represents the overall water thickness (Fig. 6, bottom panel). The hydration levels in DMPC are higher due to the presence of three methyl groups, hence influencing the hydrogen bonding. The water thickness further increases with an increase in temperature due to the Helfrich undulations. As seen in Fig. 6 (middle panel), the perturbed water layer thickness of DMPE is very constrained, suggesting that the membrane fluctuations are far less noticeable compared to DMPC. The free water layer thickness decreases with temperature for DMPC, since water uptake is dominated by the perturbed water layer (see Fig. 6, top panel). Looking at Fig. 5c (top panel), it is evident that the thickness of the bilayer, d_{HH}, shrinks as a function of temperature, due to increased disorder in the lipid chains. This study reported that while the overall water layer and perturbed water layer thickness increase with temperature, the free water layer shows an opposite trend for PC. This work is an excellent example of the crucial application of the SAXS technique in probing a model membrane.

Fernandez et al. have used SAXS to provide comprehensive insights into the effects of salt on the number of a bilayers in a MLV formed by lipid dimyristoylphosphatidylglycerol (DMPG) [62]. They showed that at low concentrations of NaCl salt, the lipid primarily forms ULVs or uncorrelated lamellae. However, at higher concentrations, it initiates the formation of giant MLVs. They concluded an increase in the number of lamellae per vesicle with an increase of salt in the vesicle dispersion. They found that above 250 mM NaCl, a clear signal of positionally correlated lamellae emerged. Despite the formation of large MLVs, these structures displayed a

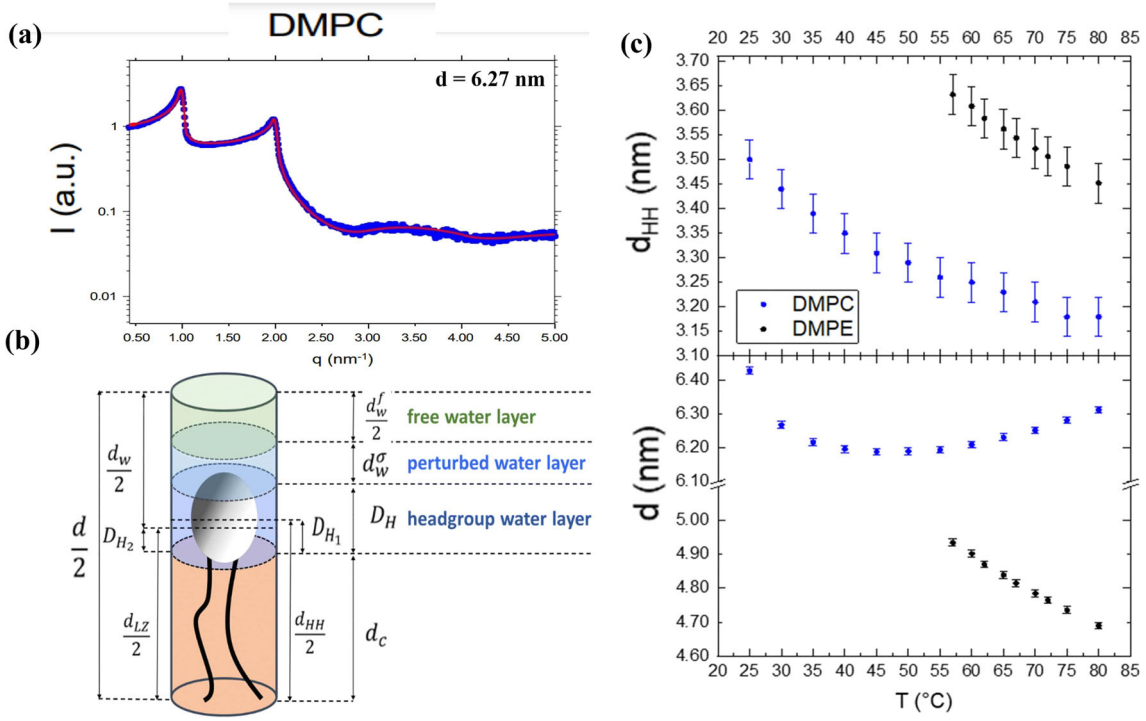

Fig. 5 **a** Global fitting of SAXS data of DMPC multi-lamellar vesicles, **b** a simplified lipid model is depicted in grey/black together with the distinct water layers associated with the (i) headgroup (blue), (ii) perturbed (light blue), and (iii) free waters (light green). The chain region is shown in light orange. **c** Behaviour of the bilayer thickness, d_{HH} (top), and overall d-spacing (bottom) as a function of temperature. Reproduced from Ref. [61] with permission from the Royal Society of Chemistry

loose correlation among bilayers. It implies that although MLVs are prevalent at high ionic strengths, the inter-bilayer correlation becomes relatively weak. There are also reports on the effects of organic salts on MLVs. In 2016, Inkeri Kontro and co-workers investigated the interaction between phosphonium-based ionic liquids (ILs) on phospholipid membranes in the presence and absence of cholesterol on vesicles of 1-Palmitoyl-2-oleoyl-sn-glycero-3-phosphocholine (POPC) [63]. From the pure lipid MLVs, two distinct peaks resulting from the coherent scattering of lipid bilayers at $q = 0.974nm^{-1}$, and $q = 1.95nm^{-1}$, corresponding to lamellar spacing of 6.45 nm were observed. With the addition of the ILs [emim][OAc] and [P_{4441}][OAc], no disordering effect on the MLV structure is observed, although, the lamellar distance decreases. Low concentrations of long-chained ILs ([P_{8881}][OAc] and [P_{14444}][OAc])shrink the lamellar distance. While the intensity of diffraction peaks remained the same or increased for [emim][OAc] and [P_{4441}][OAc], the addition of [P_{8881}][OAc] and [P_{14444}][OAc] reduced the intensity of the scattering peaks. Their study revealed that ILs that do not disrupt liposomes, but IL can decrease the lamellar spacing as a function of concentration. In contrast, the ILs that disrupt the liposomes can induce disordering in the phospholipid membrane structure. In another work, Mitra et al. investigated the effect of imidazolium-based ILs on MLVs of zwitterionic lipid [64]. They reported notable structural alterations in the model membrane models. The work demonstrates the screening of electrostatic repulsion among the bilayers containing negatively charged lipids. The findings offer critical insights into the molecular-level interactions of ILs with lipid membranes, enhancing our understanding of the biophysical properties of MLVs and their potential biomedical applications.

3 Lamellar X-ray diffraction (L-XRD)

The supported lipid multilayer (SLM) samples are prepared by drop cast method on a hydrophilic Si substrate [65–67]. In this method, slow evaporation of the solvent ensures uniform self-assembly of highly ordered stacks of lipid bilayers, forming a smectic A phase [66, 68–74]. For such a sample, the incident and scattered beam maintain specular conditions where the angle of incidence (θ_i) remains the same as the angle of reflection (θ_r). The scattered intensity is recorded as a function of θ_i, which is directly related to the z-component of the wave vector transfer (q_z), where the z-direction is along the normal of the stacks of bilayer lying horizontally on the Si-substrate. The fundamentals of this lamellar X-ray diffraction (L-XRD) technique is not different from that of the X-ray

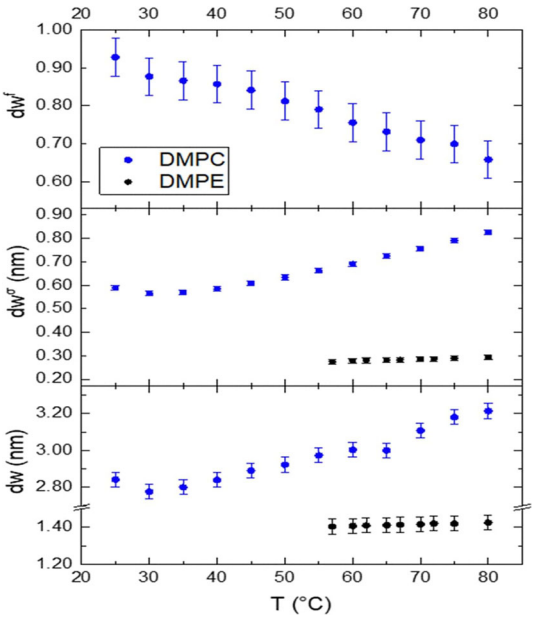

Fig. 6 The thickness of the free water layer (top), and perturbed water layer thickness (middle), and the overall water layer thickness (bottom). Reproduced from Ref. [61] with permission from the Royal Society of Chemistry

reflectivity (XRR) technique which is described in the subsequent section. However, the L-XRD provides equally spaced multiple diffraction peaks due to the correlation among the bilayers stacked on top of each other along the substrate normal [75, 76]. This is not the case in an XRR measurement which is generally performed on a single bilayer or any other thin film without a long-ranged periodicity. For the stacked bilayers, the inter-bilayer spacing (*d-spacing*) can be calculated from $d = 2\pi/q_z$ applying Bragg's law, $q_z = 4\pi \sin\theta_i/\lambda$ [77, 78].

For a periodic structure of SLM, the electron density $\rho(r)$ can be written as the convolution of a lattice function, $\rho_l(r)$, that represents the periodic lattice and a basis function, $\rho_b(r)$, [55] that describes the electron density of the basis. It is expressed as,

$$\rho(r) = \rho_l(r) \circledast \rho_b(r). \tag{13}$$

The Fourier transform of the convolution of these functions is the product of their Fourier transform. The respective transformed functions are denoted as $F_l(q)$, and $F_b(q)$ [45]. $|F_l(q)|^2$ is the structure factor, $S(q)$, which is related to the position of lattice points in the reciprocal lattice. $|F_b(q)|^2$ is the form factor, $F(q)$, defining the intensity at each lattice point. Together, the scattering intensity is given by [44], $I(q)$,

$$I(q) = \left| \int \rho(r) \exp(iq.r)\, \mathrm{d}r \right|^2 = |F_l(q)|^2 |F_b(q)|^2 = S(q)\mathbb{F}(q). \tag{14}$$

In consideration of a multilayer sample lying on the x-y plane, the $\rho(r)$ can be considered constant in the plane, while it varies periodically along $\hat{z}$ with $\rho(z) = \rho(z + nd)$. Using periodic considerations of electron density, a simplified expression for $I(q)$ [69] is,

$$I(q) = |F_b|^2 \frac{\sin^2\left(\frac{qNd}{2}\right)}{\sin^2\left(\frac{qd}{2}\right)} = |F_b|^2 N^2, \tag{15}$$

which is true for $\frac{qd}{2} = n\pi$, and 0 otherwise. $F_b(q)$ can be written as a Fourier transform of the electron density of a membrane along $\hat{z}$. This expression can be simplified based on the mirror symmetry of a model membrane system as,

$$F_b(q) = \int_{-\frac{d}{2}}^{\frac{d}{2}} \rho(z) \exp(-iq.z)\, \mathrm{d}z = \int_{-\frac{d}{2}}^{\frac{d}{2}} \rho(z) \cos qz\, \mathrm{d}z, \tag{16}$$

as the imaginary part finally becomes zero under this symmetric assumption. For such a case, the phase factor can be expressed as $+1$ or -1. The discrete form factor is related to the scattering intensity of the n^{th} order of

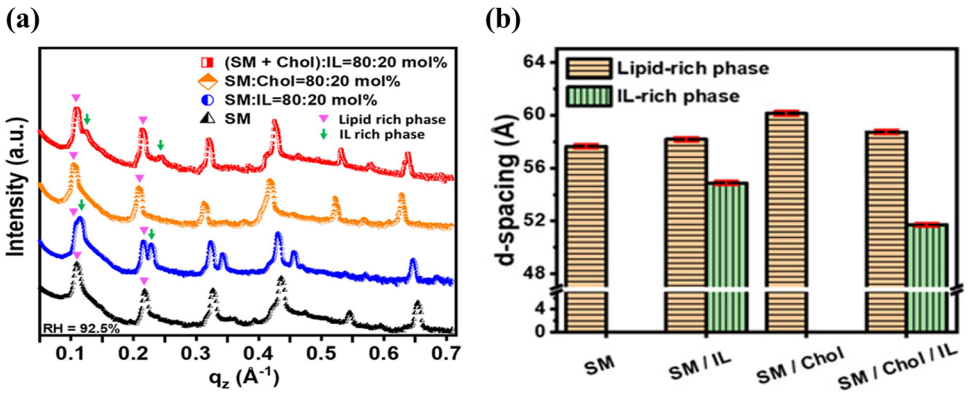

Fig. 7 **a** Scattering profile for pristine Sphingomyelin (SM) with added ionic liquid (IL) in the presence of both cholesterol and ionic liquid, **b** inter-bilayer d-spacing for pristine lipid or lipid-rich or IL-rich membrane. Adapted with permission from [79]. Copyright © 2023 American Chemical Society

the Bragg peak as $|F_n| = v_n\sqrt{nI_n}$, where v_n is ± 1, with $\sqrt{n}$ being the Lorentz correction factor. The accurate determination of this phase factor is an important task. Using the form factor amplitudes and phase factors, the electron density profile (EDP) along the lipid long axis (z-axis in Fig. 2) is obtained in arbitrary units.

Among the recent studies, Mandal and coworkers [36] have reported the structural changes in the phospholipid membrane in an SLM sample in the presence of graphene oxide (GO) nano-flakes using the expression of relative electron density as, [69, 74],

$$\rho_{\text{relative}}(z) = \frac{2}{d}\sum_n v_n n\sqrt{I_n}\cos\left(\frac{2\pi nz}{d}\right). \tag{17}$$

Through this L-XRD, they showed the coexistence of microdomains of GO-rich and GO-poor phases. it was probed that GO sheets either penetrate the hydrophobic core of the lipid bilayer or lay horizontally on the bilayer surface depending upon the degree of hydrophobic patches on the sheets. This happens due to the non-uniform oxidation of GO-flakes. In another work, with a similar approach, Hitaishi et al. showed the effect of ionic liquid (IL) on a lipid cellular membrane, using the lipid hexadecanoyl sphingomyelin [79]. As shown in Fig. 7a, the diffraction patterns for the SLM samples were different depending upon the membrane composition. The authors predicted the presence of cholesterol may reduce the adverse effects of ILs on a human cellular membrane. The ILs are much more active in a membrane in the absence of cholesterol which opens up the possibility of using them as an antimicrobial ingredient. Interestingly, the ammonium and phosphonium-based ILs are reported to induce phase-separated domains in a lipid membrane [68]. A short-range IL-rich phase with low lamellar repeat distance arising from the interdigitation is reported in the study. The L-XRD technique has been utilized to probe the mixing of lipids in an SLM system. [80]. The scattering data, shown in Fig. 8a, depicts multiple peaks due to the phase-separated domains of saturated lipids with gel phase and unsaturated lipids with fluid phase. From the electron density profiles, in Figure 8b, c, it was shown that the hybrid lipid mixes more preferentially with the unsaturated lipid than the gel phase of the saturated lipid.

To determine the phases in a lipid bilayer and the effects of a bioactive molecule on it, the oriented lamellar phases of the bilayers have been widely used. Using SAXS, Karmakar et al. determined the partial phase diagram of two binary systems, where they focused on the effects of cholesterol on the DPPC membrane [81]. They identified three lamellar phases at high hydration, namely, the fluid phase (L_α) above the main transition temperature ($\approx 42\,^\circ$C), the gel phase ($L_{\beta'}$) below pre-transition temperature ($\approx 34\,^\circ$C) and a ripple phase ($P_{\beta'}$) in between the fluid and the gel phases [82]. When cholesterol was introduced into the system, they identified the presence of "satellite" reflections in small angle regions (Fig. 9), corresponding to the modulated ripple phase (P_β). For a moderate cholesterol concentration, two sets of reflections were observed, indicating the coexistence of cholesterol-poor and cholesterol-rich gel phases above 25 °C.

4 X-ray reflectivity (XRR)

XRR is a surface-sensitive technique where electromagnetic waves are reflected from the surface of thin films as well as from interfaces between multiple media [77, 83]. As described in above section, the scattered intensity is recorded as a function of the angle of incidence in specular condition [84]. This technique has been exploited to explore the structural arrangement of lipids in a monolayer floating on a water surface or a bilayer on a substrate [85]. The EDP extracted from the XRR data provides the thickness, electron density and roughness of both the lipid head and tail region individually. [86]. This measurement also gives an insight about the attachment of additives to a specific

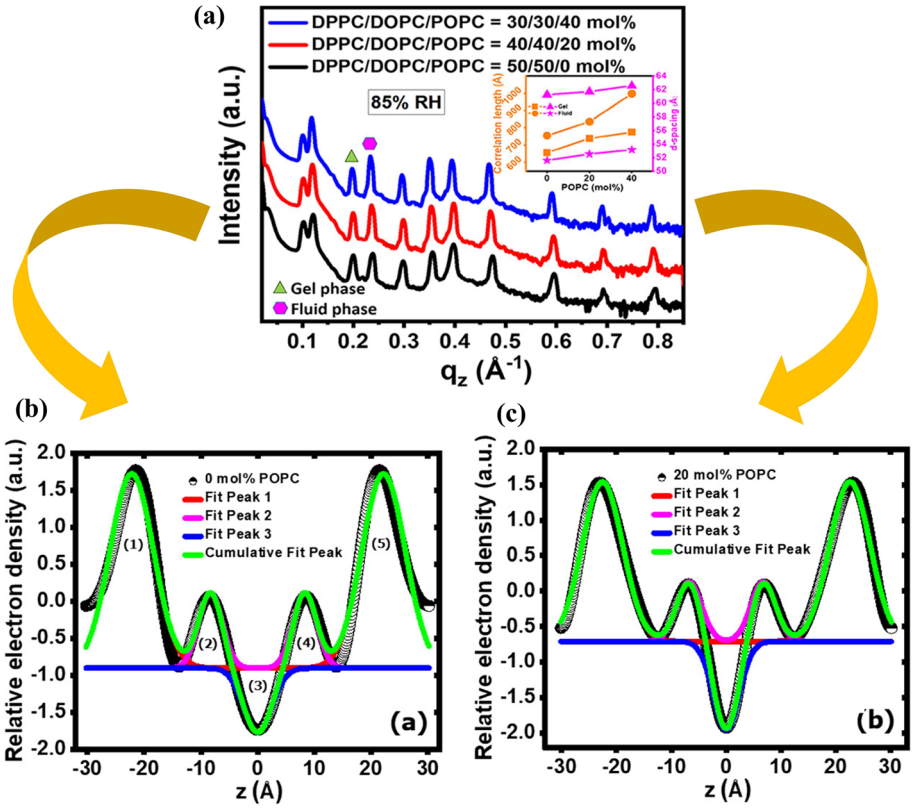

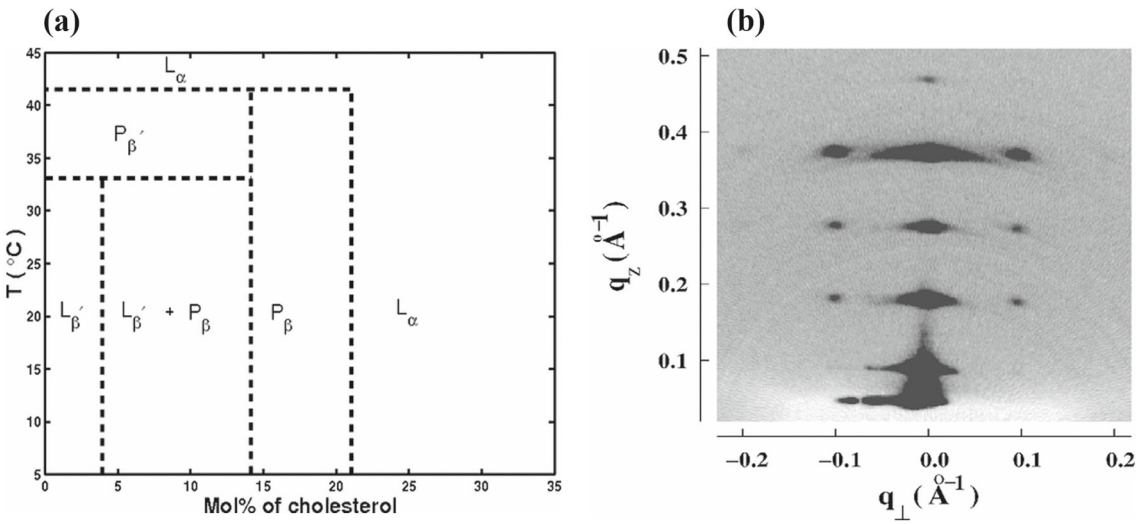

Fig. 8 **a** The L-XRD data of 2-dipalmitoyl-sn-glycero-3-phos-phocholine: 2-dioleoyl-sn-glycero-3-phosphocholine, (DPPC: DOPC) system in the presence of varied 1-palmitoyl-2-oleoyl-sn-glycero-3-phosphocholin (POPC) concentrations at 85 % relative humidity, with respective correlation length and d-spacing as inset. The corresponding electron density profile (EDP) of the mixed DPPC/DOPC system in the absence (**b**) and presence (**c**) of POPC (hybrid) lipid. Adapted with permission from Ref [80]. Copyright © 2021 American Chemical Society

Fig. 9 **a** Partial phase diagram of DPPC-cholesterol mixtures obtained from the small angle X-ray diffraction data from oriented multi bilayers. P_β is the modulated phase induced by cholesterol. **b** The small angle diffraction pattern of the P_β phase at cholesterol concentration of 15 mol% and 6 ° C temperature. Adapted with permission from Ref. [81]. Copyright ©2003 American Physical Society

region of a lipid layer. In an XRR study, the scattered intensity of a monochromatic X-ray beam from a thin film is collected as a function of the scattering angle. This intensity must be corrected to finally achieve the scattered photons from the sample [87].There are background scatterings in the specular and off-specular directions. This is corrected by collecting the background contribution only from the sample environment and eventually subtracting it from the experimental data. Since quantitative experiments are sensitive to the precise fluence distribution, the exact footprint of the X-ray beam must be considered. It depends on the incident angle, beam shape and size, and sample size [88].The correction of geometrical factors is also essential, which has been discussed by Gibaud

et al. in reference [89]. After all these corrections, the actual signal from the sample is obtained and considered for further analysis.

X-rays go through total external reflection for values of incidence angle less than the critical angle (θ_c). The expression of refractive index for X-rays is given as[90]:

$$n = 1 - \delta - i\beta \tag{18}$$

where,

$$\delta = \left(\frac{r_o \lambda^2}{2\pi}\right) N_0 \rho \sum_i x_i (Z_i + f_i') / \sum_i x_i M_i \tag{19}$$

$$\beta = \left(\frac{r_0 \lambda^2}{2\pi}\right) N_0 \rho \sum_i x_i (Z_i + f_i'') / \sum_i x_i M_i, \tag{20}$$

with r_0 being the classical radius of an electron $\left(2.818 \times 10^{-9}\ \mathrm{m}\right)$ and N_0 the Avogadro number. λ is the X-ray wavelength, ρ the density $\left(\mathrm{g/cm^3}\right)$, z_i the atomic number of the i-th atom, M_i the atomic weight of the i-th atom and x_i the atomic ratio (molar ratio) of the i-th atom. f_i' and f_i'' are the atomic scattering factors of the i-th atom (anomalous dispersion term). Here δ, the real part of the refractive index represents the atomic scattering length while the imaginary part β depends on the X-ray absorption coefficient μ through the relation $\beta = \lambda\mu/4\pi$. Furthermore, for total reflection, the value of critical angle θ_c is given by the relation $\theta_c = \sqrt{2\delta}$. Additionally, when the value of angle of incidence is increased more than the critical angle θ_c, the X-rays start penetrating into the surface and the reflectivity falls rapidly with increase in the incident angle α_i. This value of reflectivity follows the famous Fresnel's relation given by [77, 91]:

$$R_F(q_z) \approx \left| \left(q_z - \sqrt{q_z^2 - q_c^2}\right) / \left(q_z + \sqrt{q_z^2 - q_c^2}\right) \right|^2 \approx (q_c/2q_z)^4. \tag{21}$$

Here, q_c is the critical wave vector and q_z is the scattering wave vector for an α_i. The critical wave vector and the corresponding scattering vector are represented as $q_c = 4\sqrt{\pi \rho\, r_0}$ and $q_z = (4\pi/\lambda)\sin\theta$, where θ is the scattering angle. According to the Fresnel's theory, any uniform surface with multiple interfaces and thickness 'z' can be considered as a homogenous slab and the corresponding reflectivity is given as

$$r_{\text{ slab}} = \frac{r_{01} + r_{12} p^2}{1 + r_{01} r_{12} p^2}, \tag{22}$$

where, r_{01} and r_{02} are the amplitudes of reflection at interface 0 to 1 and 1 to 2, respectively and $p^2 = e^{iqz}$ is the phase factor [83]. In order to analyse the reflectivity profile, Parratt's exact recursive method is utilized. The method involves considering the medium as composed of N different layers, each layer with distinct thickness and electron densities. The layers are considered to be standing on top of an infinitely thick substrate. The reflectivity from the top of the Nth layer can be written as [83],

$$R_F(q_z) = r_{N-1,\,N} = \frac{r'_{N-1,\,N} + r'_{N,\,\infty} p_N^2}{1 + r'_{N-1,\,N} r'_{N,\,\infty} p_N^2}, \tag{23}$$

where $r_{N-1,\,N}$ and $r_{N,\infty}$ are the amplitude of reflectivity from $(N-1)$th to Nth layer and from the bottom of the Nth layer respectively. As the above discussed formalism considers the systems to have perfectly flat and sharp interfaces, an additional contribution from the roughness of surfaces is incorporated to resemble the real systems. Hence for an actual system where σ is the interfacial roughness between two different media, the total reflectivity takes the form

$$R_{\text{ rough}}\,(q_z) = R_F(q_z) e^{{q_z}^2 \sigma^2}. \tag{24}$$

4.1 XRR from lipid monolayers

Monolayer of lipid molecules provides an excellent system that can characterize the interaction of molecules, such as membrane-active proteins and peptides, with a lipid membrane [92, 93]. The monolayer can be formed at the air-water interface and this monolayer so formed can be deposited on a solid substrate. This floating layer is explored for thermodynamic properties, electrical potentials and visualizing microscopic domain [85, 94–98]. The XRR curves obtained from such a monolayer are fitted by the Parratt's recursive formalism as explained above. The analysis involves considering different boxes with a particular thickness, electron density and roughness value for modelling different regions along the surface normal. Generally, in the case of a lipid monolayer, a two-box model is preferred where one box is assigned for the lipid head region while another for the tail region [99].

In one of the earliest studies by Helm et al. in 1987, XRR measurements were performed on L-α-dipalmitoyl phosphatidylcholine (DPPC) monolayer at the air-water interface using a Langmuir trough [86]. The data eventually gave an EDP along the perpendicular to the water surface with the distinct values of length and electron density of the lipid head and tail region. They calculated the chain tilt angle in the lipid to be around 30°0. These experimental protocols and analysis methods were further extended to other observations by K. Kjaer and J. Als-Nielsen in 1988 [85]. In this detailed study, the measurements were performed on arachidic acid (C_{20}) and phospholipid dimyristoyl phosphatidic acid (DMPA) monolayers at the air-aqueous interface. The aqueous medium refers to the presence of various inorganic salts in the water subphase. The measurements revealed the modifications induced in the head region because of the salts present in water. The XRR measurements, performed on the C_{20} monolayers deposited on oxidized silicon wafer, were able to comprehend the modifications induced only to the aliphatic tail region.

Kamiński et.al. studied the effect of sterols on the incorporation of an antibiotic amphotericin B (AmB) into the DPPC monolayers at the air-water interface [100]. The chemical structures for DPPC, AmB, AmB-I (Iodine marked AmB), cholesterol and ergosterol are shown in Fig. 10a. From the corresponding scattering length densities (Fig. 10b), it was shown that mycosamine group of iodine-marked AmB (AmB-I) is located in the hydrophilic part

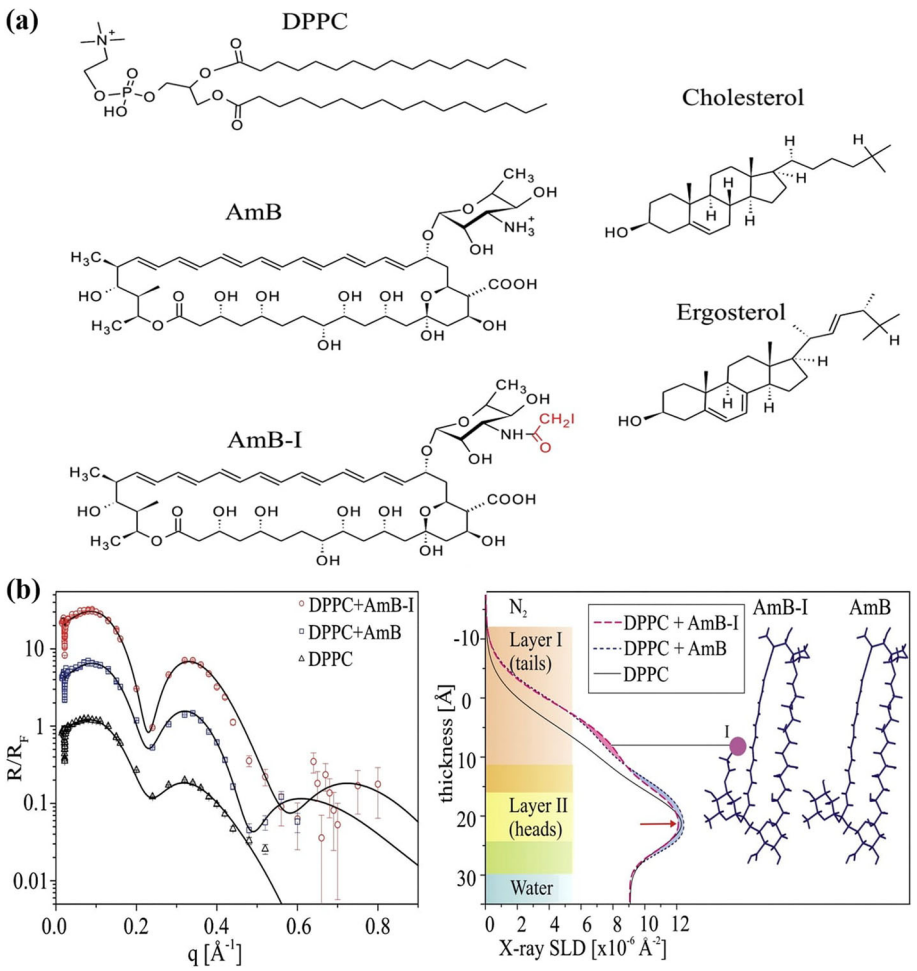

Fig. 10 **a** Chemical structures of DPPC, amphotericin B (AmB), AmB-I (Iodine marked AmB), cholesterol and ergosterol. **b** XRR curves and corresponding electron density profiles of DPPC, DPPC in presence of AmB and DPPC in presence of AmB-I.Adapted with permission from Ref. [100]

of the lipid monolayer and that AmB-I molecules are oriented with the long axis perpendicular to the surface. It was eventually concluded that both molecules and mycosamine sub-units have a similar orientation in the monolayer. Furthermore, they showed significantly larger incorporation of AmB in in the Langmuir film in presence of cholesterol or ergosterol than for the DPPC monolayer without sterols. In 2017, using XRR for supported monolayers, surface pressure—area isotherms and atomic force microscopy Giri et al. investigated the arrangement of cholesterol molecules in the 1,2-dimyristoyl-snglycero-3-phosphocholine (DMPC) and DPPC monolayers [96]. At lower concentrations of cholesterol, thinning of monolayer and subsequent lowering in the electron density of the head group region was observed. This was explained by the umbrella model along with the cholesterol condensing effect. At critical concentrations, the cholesterol molecules arrange in a way to maximize the solubility in the lipid matrix, leading to the most ordered configuration, known as the super-lattice structure. Higher amount of cholesterol produces in-homogeneous complexes with the lipid molecules. A recent paper of Mandal and coworkers showed the efficiency of XRR measurements demonstrating the self-assembly of graphene oxide (GO) nano-flakes in and around the phospholipid molecules [99]. It was observed that while GO exhibits a moderate effect on the zwitterionic monolayer, it does not affect a negatively charged phospholipid monolayer. Contrarily, the GO flakes were shown to accumulate underneath the positively charged phospholipid monolayer due to a strong electrostatic interaction resulting in increased electron density and layer thickness.

4.2 XRR from supported lipid bilayers

A supported lipid bilayer (SLB) represents the closest mimic of a biological cell membrane, which. generally, formed by vesicle fusion on a solid substrate. Researchers have also explored techniques, such as, solvent assisted lipid bilayer (SALB) and bicelle adsorption method [15]. Even Langmuir–Blodgett or Langmuir–Schaefer deposition technique has been used to eventually form a SLB [101, 102]. These SLBs have excellent compatibility with surface-sensitive measurement techniques, including acoustic, optical, plasmonic, and electrochemical sensors along with fluorescence and atomic force microscopy [15]. In order to perform the XRR measurements, customized sample cells are used with well defined holding space for aqueous environment to maintain the lipid bilayer structure. The data are collected in exactly the same way of monolayer as discussed above. The collected reflectivity curves are fitted again fitted by the Parratt's recursive formalism. The difference in the analysis comes in modeling the lipid layers by the increasing the number of boxes. In the case of a SLB, a multi-box model is preferred where individual boxes are assigned to two different heads of lipids and their tails. In some cases, a oxide layer on the solid substrate and a water cushion below the bilayer are considered to achieve the best fit to the XRR data.

In 2006, Miller et al. successfully demonstrated XRR measurements on phospholipid membrane SLBs at the solid–liquid interface using a high resolution synchrotron radiation source for two different membrane systems which were formed by vesicle fusion [103]. The XRR curves were fitted considering a four-box model using the Parratt's algorithm. The obtained scattering length densities were in excellent agreement with earlier explored neutron reflectivity results. In another study, Watkins et. al, demonstrated XRR study on bilayers formed on polymer cushion [104] where the bilayers were deposited on a quartz substrate using Langmuir-Blodgett and Langmuir Schaefer method. A similar system of cushioned bilayers was utilized by Bhattacharya and co workers to study the interaction of an imidazolium based ionic liquid with DPPC bilayers [105]. The cushioning in this particular case was provided by the spin coated poly (acrylic acid) (PAA) layer on the surface of silicon wafers. The experiments were performed at gel and fluid phases of the lipids to characterize the changes induced by the ionic liquid in the respective phases. In both the phases, a substantial decrease in the bi-layer thickness was observed with simultaneous increase in the electron density of the lipid bilayer, indicating strong perturbations in the self-assembled structure induced by the ionic liquid. Giri et. al studied the behaviour of polymer cushion-supported membrane by replacing bulk water by a relative humidity (RH) environment [106]. (see Fig. 11a). The lipid bilayers were deposited on a silicon wafer treated with a with layer of (3-Aminopropyl) triethoxysilane (APTES) and further cushioned by a PAA layer (Fig. 11b). XRR was performed from the SLBs of two representative phospholipids, phosphocholine (PC) and phosphoethanolamine (PE), in their fluid and gel phase, respectively. The integrity of the bilayer structure remained intact over hours, allowing sufficient time for multiple X-ray measurements. In comparison to the water column, the introduction of the RH environment helped in accessing the bilayer structural features (Fig. 12b) without being perturbed by the background signals from the traditional water column. For XRR measurements these modifications induced in the system smoothly enhanced the dynamic range approximately by 100-fold and the structural resolution by 2-fold.

5 Grazing incidence X-ray diffraction (GIXD)

GIXD is a X-ray scattering technique that can probe the in-plane organization of lipids in a monomolecular layer or ultrathin films of multiple layer [98, 107]. In the measurement, X-rays are impinged on the sample surface at a grazing incidence angle below the critical angle of total external reflection, eventually leading to an evanescent

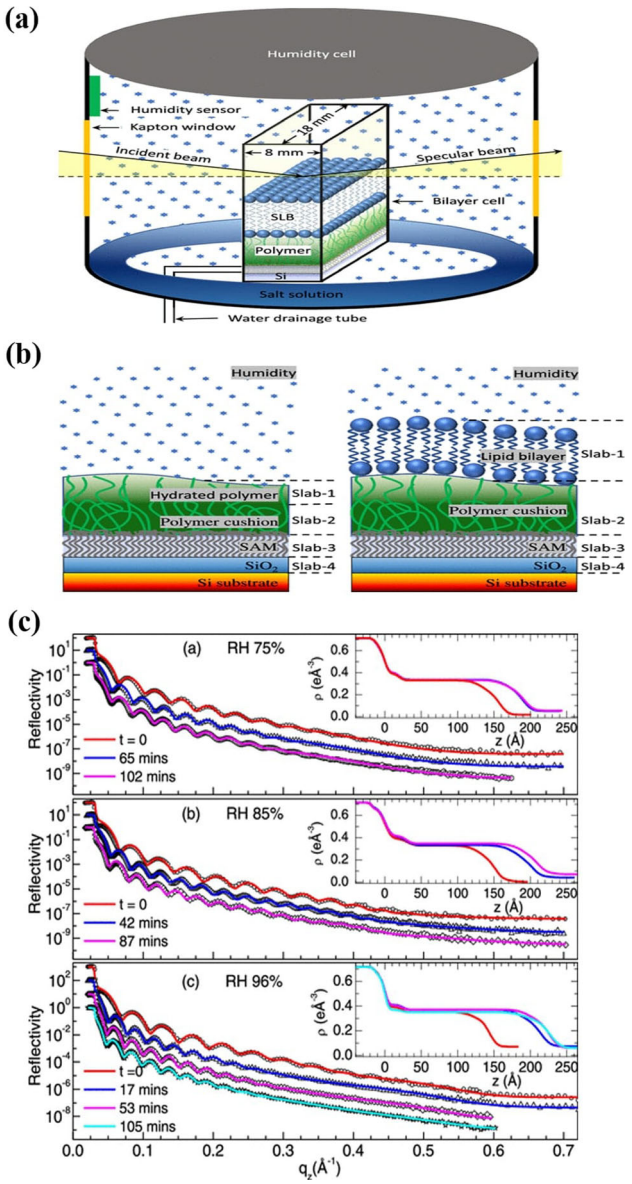

Fig. 11 **a** Schematic representation of the humidity cell consisting of a lipid bilayer cell at the center along with the scattering geometry used in the X-ray measurements. **b** Schematics showing a stack of slabs,for the polymer cushion and polymer cushion-supported lipid bilayer under the relative humidity used for model fitting of the XRR profiles. **c** Time response XRR data obtained from polymer cushion layers at **a** RH 75%, **b** RH 85%, and **c** RH 96%. Adapted with permission from Ref. [106].Copyright © 2022 American Chemical Society

wave propagating parallel to the surface. Since the perpendicular component of waves dampens exponentially [108], this evanescent wave is scattered only from the first few layers of any material. This results in an exceptionally increased surface sensitivity as the incident, reflected and the transmitted wave fields couple coherently at the surface [109]. The ability of GIXD to probe lattice planes that are almost perpendicular to the surface allows scattering experiments for organic surfaces with very low scattering volume [110].

In GIXD techniques, the vertical component (q_z) can be separately measured, while the horizontal component which includes q_x and q_y, the in-plane scattering vectors, are measured as (q_{xy}) given by [26, 99],

$$q_{xy} = \sqrt{q_x^2 + q_y^2} \tag{25}$$

The vertical component for angle of incidence (α_i) and the angle of reflection α_r can be given as:

$$q_z = k(\sin\alpha_i + \sin\alpha_r) \tag{26}$$

For the scattering angle 2θ, the horizontal component is given as:

$$q_{xy} = k\sqrt{(\cos^2\alpha_i + \cos^2\alpha_f - 2\cos\alpha_i\cos\alpha_f\cos 2\theta)}, \tag{27}$$

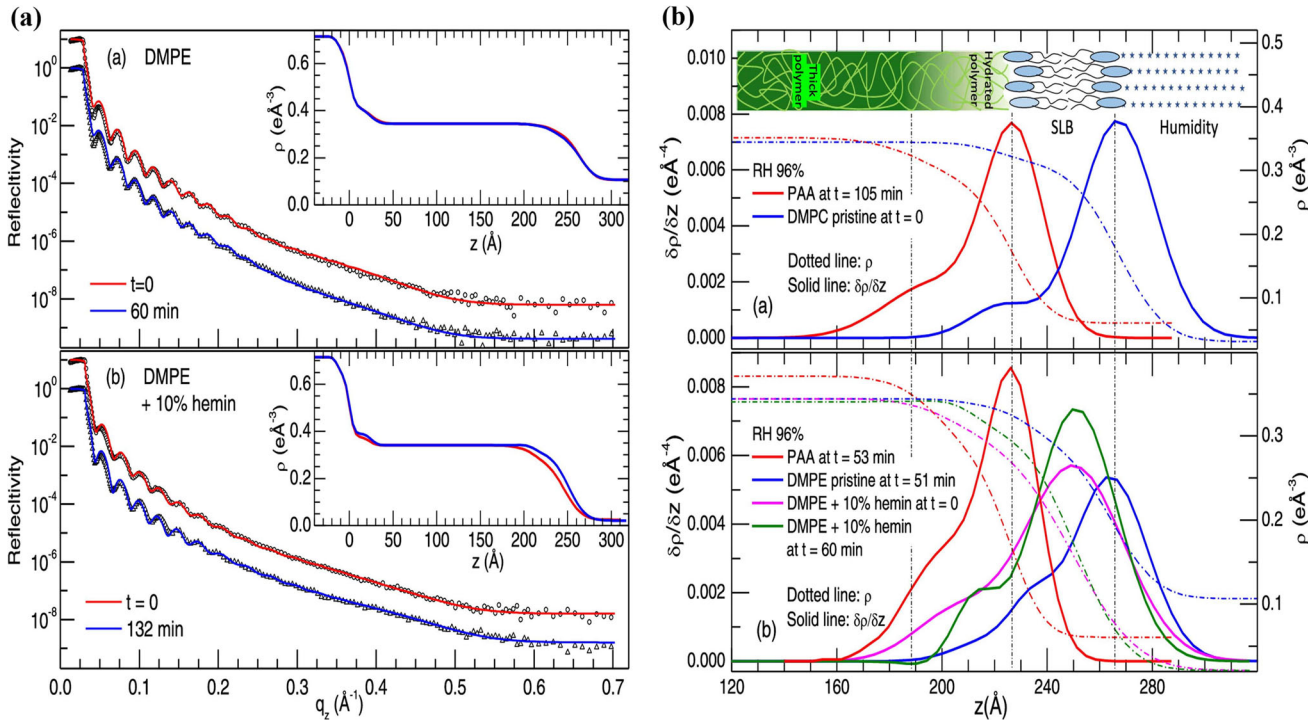

Fig. 12 **a** Time-response XRR data and EDPs (inset) obtained from the pristine DMPE SLB and DMPE SLB with 10 mol% hemin at RH96%. **b** Enhanced SLB features: Part of EDPs (dotted lines) close to the humidity interface and corresponding differentiated EDPs obtained from pristine DMPC and DMPE SLB with and without hemin along with the hydrated polymer(red curves) under a 96%RH environment.Adapted with permission from Ref. [106].Copyright © 2022 American Chemical Society

or

$$q_{xy} = 2k \sin\theta = (4\pi/\lambda) \sin\theta, \tag{28}$$

where, λ is the wavelength of incident X-rays. The position of the q_{xy} peaks gives the 2D lattice repeat distance as [111, 112]:

$$d_{hk} = 2\pi/q_{xy}^{hk}, \tag{29}$$

where, h and k are the Miller indices required to calculate the unit cell parameters. The 2D crystalline coherence length (L_{xy}) can be calculated from the Scherrer formula [113, 114]

$$L_{xy} = (0.9 \times 2\pi)/\text{FWHM}_{\text{intrinsic}}\,(q_{xy}), \tag{30}$$

where the full width at half maxima (FWHM) of a peak is calculated from,

$$\text{FWHM}_{\text{intrinsic}}\,(q_{xy}) = \sqrt{\text{FWHM}_{\text{expt}}\,(q_{xy})^2 - \text{FWHM}_{\text{reso}}\,(q_{xy})^2}, \tag{31}$$

with $\text{FWHM}_{\text{expt}}(q_{xy})$ being the value obtained from the Lorentzian fit to the respective peak, and the $\text{FWHM}_{\text{reso}}\text{reso}(q_{xy})$ is the instrument resolution. The presence of one out-of-plane Bragg rod gives rise to a molecular tilt (τ) toward the nearest neighbor (NN) which is calculated by

$$\tan\tau = \frac{(q_z^{\text{d}})}{\sqrt{(q_{xy}^{\text{d}})^2 + (q_{xy}^{\text{n}})^2}}. \tag{32}$$

Here, "d" and "n" denote the "degenerate" and "non-degenerate" peaks, respectively.

5.1 GIXD from lipid monolayers

GIXD measurements can be performed on the lipid monolayers formed at the air–water interface or deposited on a substrates. The diffraction peaks are fitted using a Lorentz function to figure out the 2D lattice formed by the lipid molecules in the lipid layer. Furthermore, the obtained Bragg rods reveal information about tilt angle (τ) and coherence length (L_c) of the alkyl tails. In 2004, Wang et al. observed the structural changes induced by human serum albumin (HAS) in the monolayers of small ionic L-α-dipalmitoyl phosphatidic acid (DPPA), large ionic L-α-dipalmitoyl-phosphatidyl-L-serine (DPPS) and zwitterionic L-α-distearoyl- phosphatidylcholine (DSPC), at the air-water interface [115]. The pronounced changes observed in the tilt angles of anionic DPPA and DPPS monolayers indicated that coupling of HAS to the monolayer is being governed by electrostatics. Another study by Neville and coworkers in 2008 showed the interaction of DPPC, DPPG and lipid A monolayers with an antimicrobial peptide protegrin-1 (PG-1) [116]. It was observed that the peptide molecules had preferential interactions with anionic lipids as governed by electrostatics. There was an additional peptide layer adsorbed just below the head group region of both the lipids DPPG and lipid A. The disappearance of Bragg peaks after introduction of PG-1 to the DPPG system confirmed the monolayer disruption in this particular case.

In a recent study, Behyan et. al investigated the self-assembly of cationic silica Levasil 200 S and anionic silica Bindzil 30/360 nanoparticles in and around monolayers of DPPC, mixtures of DPPC and 1,2-dilauroyl-sn-glycero-3-phosphocholine (DLPC) or 1-palmitoyl-2-oleoyl-sn-glycero-3-phosphoglycerol (POPG), and Infasurf (a clinical lung surfactant formulation) [117]. Through XRR and GIXD, it was shown that anionic nanoparticles interact with the lipid head groups, but only induce a small change in the lipid head group and alkyl chain organization and orientation. Contrarily, for the case of anionic lipids, a substantial reduction in the chain tilt angle was induced by the cationic silica nanoparticles. This indicated that the pulmonary function can be hampered by even very low concentration of cationic nanoparticles as they impact the mechanical properties of surfactant films. In biological systems, the interaction among the macromolecules is strongly influenced by the presence of ions. In particular, the presence of ions in the aqueous medium plays a vital role in modulating the structure and dynamics of a lipid membrane. The process of exposing the model membranes to various types of ions is itself an exciting field of research [118]. Recent studies from the Karmakar group have shed light on the assembly and interaction of the ions, with varying valency with such membranes [119, 120]. They showed that the Gouy-Chapman theory fails in the range of high electrolyte concentration. Further, the affinity of anions to a positively charged membrane was found to be descending in the order of size of the ions. In 2012, using XRR and GIXD, Ghosh et al. carried out a quantitative study of the structure of lipid monolayers of defined compositions in presence of Ca^{2+} ions [35]. In this regard, measurement of two main structural parameters, i.e., the tilt of the acyl chains and the area per lipid, were performed. It was concluded that Ca^{2+} induces compaction in the film by reducing both the area per molecule and the chain tilt angle. However, this trend is partially counteracted by incubation of synaptic vesicles with the monolayer. Here, the Ca^{2+} ions effectively bridge up the anionic phosphate groups of the lipid molecules and compact the lipids, eventually leading to the packing of lipids into a smaller unit cell.

There are experiments where the GIXD has been combined simultaneously with other experimental techniques. Bera et al. conducted GIXD with rheology to explore in situ membrane lattice structure in DPPC-alamethicin monolayers under nonequilibrium state [121]. It was shown that the 2D crystallites grow bigger by the merging of crystalline domains under shear. Further, the peptide is found to be unable to bind with the DPPC head group in presence of shear. Interestingly, in case of mixed monolayer, there was indication of phase separated domain during flow.

While the works discussed above explain the usefulness of GIXD to explore a lipid monolayer, it would be further beneficial to couple it with with other technique. The coupling of GIXD with rheology by Bera et.al. can work as a benchmark to develop systems for performing these kinds of complex measurements.

5.2 GIXD from lipid bilayers

GIXD measurements on SLBs provide high resolution structural information about the packing of lipids and can eventually define the role of leaflet-leaflet interactions in assembling lipids in a membrane. A study by Watkins et al. in 2009 demonstrated the diffraction of X-rays from SLBs of DPPC [122]. They showed that SLBs of DPPC formed by the Langmuir-Blodgett-Schaefer technique have less disorder in the inner leaflet when compared to the SLBs formed by the vesicle fusion method. The GIXD measurements affirmed that the in-plane and out-of-plane structure of a single bilayer was very analogous to multilamellas. In 2014, same group published another paper which described the differences between packing of lipids in a monolayer, supported bilayer, and a in a multilayer film [123]. They deposited multiple SLBs at different surface pressures using the Langmuir-Blodgett-Schaefer (LBS) technique. They concluded that the SLBs deposited by LBS technique at 38 mN/m surface pressure resemble those formed by the vesicle fusion method. It was also observed that the outer leaflet templates on the inner leaflet due to the coupling between opposite lipid acyl chains which in turn induces the acyl chain tilt.

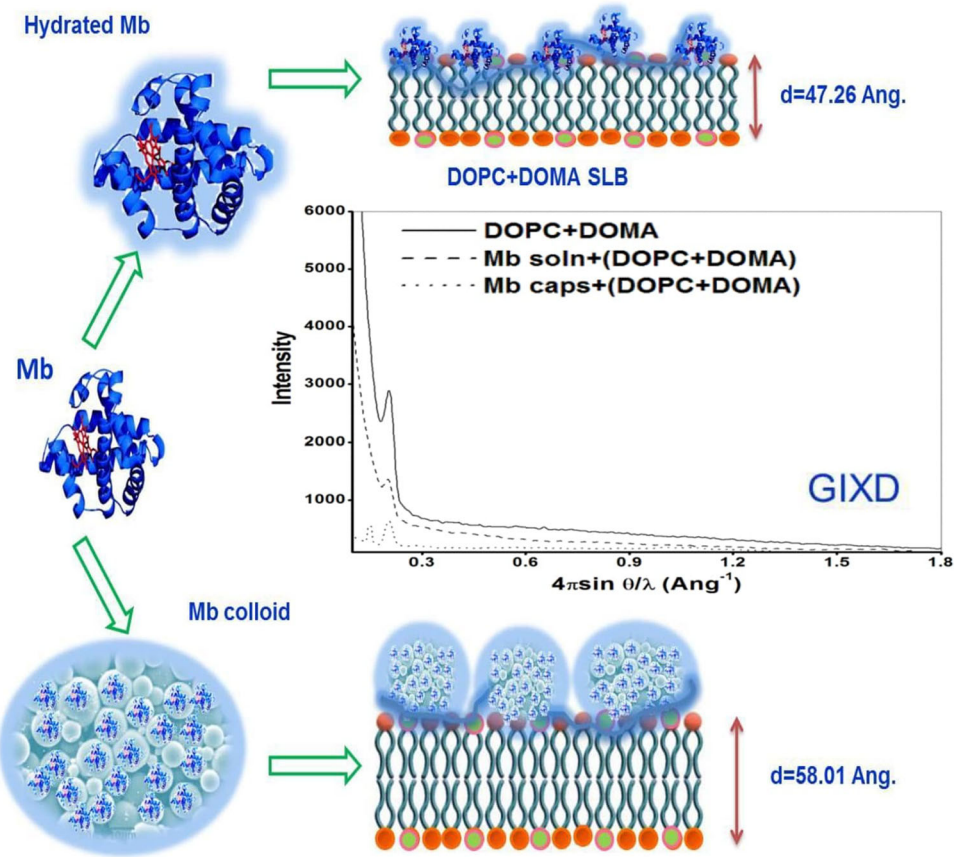

Fig. 13 The spreading and subsequent changes in the bilayer spacing due to the adsorption of the hydrated myoglobin (Mb) in solution and in the form of colloids with the corresponding GIXD data. Adapted with permission from Ref. [124]

Dhanasekaran and group studied the effect of Myoglobin (Mb) in solution and colloidal forms on the SLBs of electrically neutral DOPC, cationic dioctadecyl dimethylammonium bromide (DOMA) and mixture of DOPC and DOMA [124]. The SLBs were supported by quartz surface and silicon dioxide substrates. When Mb is used in the solution form, the bilayer head group remains nearly undisturbed for neutral SLBs and the mixture case. In case of Mb in colloidal form, an increase in head group thickness with neutral, and decrease in the case of mixture is observed. While for neutral lipids these changes existed due to the unsaturation in the alkyl tails, the cationic SLBs displayed this behaviour due to more entrained water in the system. A schematic showing the spreading and subsequent changes in the bilayer spacing due to the adsorption of the hydrated Mb in solution and in the form of colloids with the corresponding GIXD data is shown in Fig. 13.

The presence of a solid substrate under SLBs can limit their potential applications. In this regard, a recent advancement has been made by Pusterla et al. in 2022. They were able to adsorb lipid bilayers to a lipid monolayer dispersed at the air-water interface [125]. This was done through the fusion of small unilamellar vesicles (SUV) to the lipid monolayer by means of electrostatic interaction. Using ellipsometry, X-ray scattering techniques and X-ray fluorescence a comprehensive structural picture of surface-adsorbed bilayer was realized. The bilayer fluid phase and the in chain-ordered phases were characterized by GIXD. The chain ordering was found to be significantly different from that in a regular Langmuir monolayer. This development of surface-adsorbed lipid bilayers opens up a new possibility for future studies involving the formation of protein or glycolipid functionalized domains.

6 Limitations, outlook, and future prospects

Over last few decades, there has been tremendous progress in probing the structural details of model lipid membranes, in their various forms, due to the advancement in X-ray scattering techniques. Especially, the new generation synchrotron sources, with X-ray beam that can be tuned according to the requirement of sample geometry and environment, have opened up immense possibilities. However, one of the most discussed limitations of these high brilliance X-ray sources is the radiation damage. High flux and focused X-ray photons can damage the chemical bonds in organic materials, generating faulty scattering data. For lipids, this high flux can change the ordering of molecules in a particular phase or can lead to a complete phase transition induced by beam heating. Furthermore,

the higher-order lamellar reflections can broaden and lose intensity, eventually leading to the development of higher diffused scattering [126]. To avoid such issues, a radiation damage test is an important step, and it is done by repeating a particular type of scan. Optimized beam flux, exposure time, lateral transition of exposure spot, continuous exchange of surrounding medium etc. are a few remedial steps that can be followed in an X-ray scattering experiment on biological materials at a synchrotron source. Therefore, one has to wisely choose the experimental setup along with the time of beam exposure. Another limitation is the production of average structure of a sample over a large sample area. Recently, lots of efforts are being employed to achieve nano-focused beam to probe local area of a sample to explore the natural heterogeneity. Moreover, X-ray scattering is not element-specific, and the proximity of electron densities of different elements of lipid to water may provide ambiguous structural details of a model membrane. On the other hand, in neutron scattering, the scattering lengths not only change from element to element but also differ between the isotopes of the same element. Neutron scattering has this significant advantage, which may be utilized in soft materials where such an alteration of isotopes is easily feasible [22]. Eventually, this allows to probe the structure and dynamics of the complex membrane, highlighting the contributions from individual components [127]. Nonetheless, a few technique-specific comments and future prospects about the X-ray scattering techniques are discussed below.

(i) Although, SAXS has been widely used for probing MLVs and ULVs, it may still be improved in various fronts, such as experimental design, data analysis, and instrumentation. It is required to enhance the electron density contrast between the vesicle and the surrounding medium to improve the visibility of signal from vesicles in a scattering pattern. One could develop improved sample preparation methods to ensure repeatability and homogeneity, reducing the polydispersity in size and structure. Furthermore, development of efficient and user friendly analysis methods, to quantify the structural parameters for anisotropic/ asymmetric membrane samples, is necessary to popularize this important technique. Implementation of machine learning algorithms for more efficient and accurate data analysis would be the next endeavour.

(ii) While L-XRD can provide information about the repeat distance, packing, and orientation of the lipid layers, it does not provide information about the in-plane organization of lipids. The sensitivity to hydration of the lipid membrane poses a limitation. For this technique, a sample has to be highly oriented with a well-defined periodic structure. A model membrane with low bending rigidity may cause high out-of-plane fluctuation producing disordering in the stack. Despite these limitations, this technique remains a valuable tool for studying the structural characteristics of planar SLMs, providing important insights into their organization and properties.

(iii) Although XRR measurements on lipid monolayer or bilayer provide a great deal of information about the structural arrangements of lipid molecules, additional progress can be made in the direction of coupling these measurements with other characterization techniques. Parallelly, further improvements in experimentation and data analysis can be made through developing automated set-ups utilizing the swiftly growing applications of artificial intelligence.

Comprehensively, SLBs have been a perfect contender for the biomimetic explorations and have been used for reflectivity measurements, be it neutron reflectivity or X-ray reflectivity. However, the presence of the solid support comes with its own disadvantages as it limits the out of plane fluctuation of the membrane. These SLBs cannot be exploited for exploring spectroscopic techniques as well as surface rheological measurements. Free standing lipid bilayers either in solution or at an interface, is the solution which has to be established in a detailed manner.

(iv) Generally the GIXD signal generated from lipids in mono-, bi- or multi-layer cases is quite poor. In many instances it becomes difficult to figure out the in-plane lattice from the one or two diffraction peaks. The electron density contrast between the hydrocarbon chain and the surrounding water medium is weak. One has to enhance the photon flux to receive better scattering signal which inherently increases the chances of radiation damage. Therefore, new avenues for efficient GIXD measurements have to be explored.

Acknowledgements A.S. and D.K. are thankful to Shiv Nadar Foundation for the research fellowship. S.K.G. acknowledges the financial support received from UGC-DAE CSR (Mumbai Centre, CRS/2022-23/1235) for conducting the research.

Data availability statement No data associated in the manuscript.

References

1. R.B. Gennis, *Biomembranes: Molecular Structure and Function* (Springer Science & Business Media, 2013)
2. G.L. Nicolson, The Fluid-Mosaic Model of Membrane Structure: still relevant to understanding the structure, function and dynamics of biological membranes after more than 40 years. Biochim. Biophys. Acta (BBA)-Biomembr. **1838**(6), 1451–1466 (2014)
3. L.J. Pike, The challenge of lipid rafts. J. Lipid Res. **50**, S323–S328 (2009)
4. S. Jonathan Singer, G.L. Nicolson, The Fluid Mosaic Model of the Structure of Cell Membranes: cell membranes are viewed as two-dimensional solutions of oriented globular proteins and lipids. Science **175**(4023), 720–731 (1972)

5. K. Simons, E. Ikonen, Functional rafts in cell membranes. Nature **387**(6633), 569–572 (1997)
6. D. Lingwood, K. Simons, Lipid rafts as a membrane-organizing principle. Science **327**(5961), 46–50 (2010)
7. J.D. Nickels et al., Lipid rafts: buffers of cell membrane physical properties. J. Phys. Chem. B **123**(9), 2050–2056 (2019)
8. M. Venturoli et al., Mesoscopic models of biological membranes. Phys. Rep. **437**(1–2), 1–54 (2006)
9. "Challenges in the theoretical investigations of lipid membrane configurations". Chin. Phys. B **22**(2), p. 028701 (2013). https://doi.org/10.1088/1674-1056/22/2/028701
10. Y. Gerelli, Chapter Three—exploring interactions between lipid membranes and nanoparticles through neutron and X-ray reflectometry techniques". In *Advances in Biomembranes and Lipid Self-Assembly*. Ed. by Aleš IgliÄ, Michael Rappolt, and Patricia Losada-Pérez. Vol. 38. Advances in Biomembranes and Lipid Self-Assembly. Academic Press, pp. 37–61 (2023). https://doi.org/10.1016/bs.abl.2023.07.001. https://www.sciencedirect.com/science/article/pii/S2451963423000016X
11. H.I. Okur, O.B. Tarun, S. Roke, Chemistry of lipid membranes from models to living systems: a perspective of hydration, surface potential, curvature, confinement and heterogeneity. J. Am. Chem. Soc. **141**(31), 12168–12181 (2019)
12. S.L. Veatch, S.L. Keller, Seeing spots: complex phase behavior in simple membranes. Biochim. Biophys. Acta (BBA)-Mol. Cell Res. **1746**(3), 172–185 (2005)
13. J. Korlach et al., Characterization of lipid bilayer phases by confocal microscopy and fluorescence correlation spectroscopy. Proc. Natl. Acad. Sci. **96**(15), 8461–8466 (1999)
14. A. Kress et al., Mapping the local organization of cell membranes using excitation-polarization-resolved confocal fluorescence microscopy. Biophys. J . **105**(1), 127–136 (2013)
15. J.A. Jackman, N.-J. Cho, Supported lipid bilayer formation: beyond vesicle fusion. Langmuir **36**(6), 1387–1400 (2020)
16. J.F. Nagle et al., Structure of gel phase DPPC determined by X-ray diffraction. Biophys. J . **116**(3), 225a (2019)
17. B. Fadeel, D. Xue, The ins and outs of phospholipid asymmetry in the plasma membrane: roles in health and disease. Crit. Rev. Biochem. Mol. Biol. **44**(5), 264–277 (2009)
18. A.J. Guillot et al., Skin drug delivery using lipid vesicles: a starting guideline for their development. J. Control. Release **355**, 624–654 (2023)
19. A. Morshed et al., Mechanical characterization of vesicles and cells: a review. Electrophoresis **41**(7–8), 449–470 (2020)
20. G.P. Kumar, P. Rajeshwarrao, Nonionic surfactant vesicular systems for effective drug delivery–an overview. Acta Pharm. Sin. B **1**(4), 208–219 (2011)
21. R. Dimova, Giant vesicles and their use in assays for assessing membrane phase state, curvature, mechanics, and electrical properties. Annu. Rev. Biophys. **48**, 93–119 (2019)
22. T.A. Harroun et al., Neutron and X-ray scattering for biophysics and biotechnology: examples of self-assembled lipid systems. Soft Matter **5**(14), 2694–2703 (2009)
23. G. Pabst et al., Applications of neutron and X-ray scattering to the study of biologically relevant model membranes. Chem. Phys. Lipid. **163**(6), 460–479 (2010)
24. M.A. Kiselev, D. Lombardo, Structural characterization in mixed lipid membrane systems by neutron and X-ray scattering. Biochim. Biophys. Acta (BBA)-Gener. Sub. **1861**(1), 3700–3717 (2017)
25. F.A. Heberle et al., Model-based approaches for the determination of lipid bilayer structure from small-angle neutron and X-ray scattering data. Eur. Biophys. J. **41**, 875–890 (2012)
26. S.K. Ghosh et al., In vitro study of interaction of synaptic vesicles with lipid membranes. New J. Phys. **12**(10), 105004 (2010)
27. R.S. Shirazi et al., Structural evolution of environmentally responsive cationic liposome-DNA complexes with a reducible lipid linker. Langmuir **28**(28), 10495–10503 (2012)
28. N.F. Bouxsein et al., Two-dimensional packing of short DNA with nonpairing overhangs in cationic liposome-DNA complexes: from onsager nematics to columnar nematics with finite-length columns. J. Am. Chem. Soc. **133**(19), 7585–7595 (2011)
29. R. Beck et al., Gel-expanded to gel-condensed transition in neurofilament networks revealed by direct force measurements. Nat. Mater. **9**(1), 40–46 (2010)
30. R. Winter, Synchrotron X-ray and neutron small-angle scattering of lyotropic lipid mesophases, model biomembranes and proteins in solution at high pressure. Biochim. Biophys. Acta (BBA)-Protein Struct. Mol. Enzymol. **1595**(1–2), 160–184 (2002)
31. M. Rappolt et al., Phospholipid mesophases at solid interfaces: in-situ X-ray diffraction and spin-label studies. Adv. Coll. Interface. Sci. **111**(1–2), 63–77 (2004)
32. N.W. Schmidt et al., Criterion for amino acid composition of defensins and antimicrobial peptides based on geometry of membrane destabilization. J. Am. Chem. Soc. **133**(17), 6720–6727 (2011)
33. M. Kornreich, R. Avinery, R. Beck, Modern x-ray scattering studies of complex biological systems. Curr. Opin. Biotechnol. **24**(4), 716–723 (2013)
34. O. Szekely et al., The structure of ions and zwitterionic lipids regulates the charge of dipolar membranes. Langmuir **27**(12), 7419–7438 (2011)
35. S.K. Ghosh et al., Measuring Ca2+-induced structural changes in lipid monolayers: implications for synaptic vesicle exocytosis. Biophys. J . **102**(6), 1394–1402 (2012)
36. P. Mandal et al., Unravelling the structural changes of phospholipid membranes in presence of graphene oxide. Appl. Surf. Sci. **539**, 148252 (2021)

37. P.V. Konarev et al., Restoring structural parameters of lipid mixtures from small-angle X-ray scattering data. J. Appl. Crystallogr. **54**(1), 169–179 (2021)
38. P. Heftberger et al., Global small-angle X-ray scattering data analysis for multilamellar vesicles: the evolution of the scattering density profile model. J. Appl. Crystallogr. **47**(1), 173–180 (2014)
39. C.V. Kulkarni, Lipid crystallization: from self-assembly to hierarchical and biological ordering. Nanoscale **4**(19), 5779–5791 (2012)
40. S.F. Fenz, K. Sengupta, Giant vesicles as cell models. Integr. Biol. **4**(9), 982–995 (2012)
41. A.D. Bangham, M.M. Standish, J.C. Watkins, Diffusion of univalent ions across the lamellae of swollen phospholipids. J. Mol. Biol. **13**(1), 238-IN27 (1965)
42. D.D. Lasic, *Liposomes: from physics to applications* (Elsevier, 1993)
43. T.M. Allen, P.R. Cullis, Liposomal drug delivery systems: from concept to clinical applications. Adv. Drug Deliv. Rev. **65**(1), 36–48 (2013)
44. A. Guinier, *X-ray Diffraction in Crystals, Imperfect Crystals, and Amorphous Bodies* (Courier Corporation, 1994)
45. R. Guinebretière, *X-ray Diffraction by Polycrystalline Materials* (Wiley, 2013)
46. M.R. Brzustowicz, A.T. Brunger, X-ray scattering from unilamellar lipid vesicles. J. Appl. Crystallogr. **38**(1), 126–131 (2005)
47. J. Gummel et al., Concentration dependent pathways in spontaneous self-assembly of unilamellar vesicles. Soft Matter **7**(12), 5731–5738 (2011)
48. V. Chappa et al., The effect of polydispersity, shape fluctuations and curvature on small unilamellar vesicle small-angle X-ray scattering curves. J. Appl. Crystallogr. **54**(2), 557–568 (2021)
49. I. Grillo, Applications of stopped-flow in SAXS and SANS. Curr. Opin. Colloid Interface Sci. **14**(6), 402–408 (2009)
50. T. Narayanan et al., Probing the self-assembly of unilamellar vesicles using time-resolved SAXS. Advances in planar lipid bilayers and liposomes, vol 20 (Academic Press, 2014), pp. 171–196
51. K. Komorowski et al., Vesicle adhesion and fusion studied by small-angle X-ray scattering. Biophys. J . **114**(8), 1908–1920 (2018)
52. S. Castorph et al., Structure parameters of synaptic vesicles quantified by small-angle x-ray scattering. Biophys. J . **98**(7), 1200–1208 (2010)
53. A.V. Rawlings et al., Stratum corneum moisturization at the molecular level. J. Investig. Dermatol. **103**(5), 731–740 (1994)
54. Y. Sun et al., Recent advances in structural characterization of biomacromolecules in foods via small-angle X-ray scattering. Front. Nutr. **9**, 1039762 (2022)
55. R. Hosemann, S.N. Bagchi, Calculation of electron-density distribution in crystals with the help of convolution operations. Nature **171**(4357), 785–787 (1953)
56. A. Caillé, Remarques sur la diffusion des rayons X dans les smectiques. CR Acad. Sci. Serie B **274**, 891–893 (1972)
57. R. Zhang et al., Small-angle x-ray scattering from lipid bilayers is well described by modified Caillé theory but not by paracrystalline theory. Biophys. J . **70**(1), 349–357 (1996)
58. R. Zhang, R.M. Suter, J.F. Nagle, Theory of the structure factor of lipid bilayers. Phys. Rev. E **50**(6), 5047 (1994)
59. M.C. Wiener, R.M. Suter, J.F. Nagle, Structure of the fully hydrated gel phase of dipalmitoylphosphatidylcholine. Biophys. J . **55**(2), 315–325 (1989)
60. G. Pabst et al., Structural information from multilamellar liposomes at full hydration: full q-range fitting with high quality x-ray data. Phys. Rev. E **62**(3), 4000 (2000)
61. G. Vancuylenberg et al., Planar confined water organisation in lipid bilayer stacks of phosphatidylcholine and phosphatidylethanolamine. Soft Matter **19**, 5179–5192 (2023)
62. R.M. Fernandez et al., Influence of salt on the structure of DMPG studied by SAXS and optical microscopy. Biochim. Biophys. Acta (BBA)-Biomembr. **1778**(4), 907–916 (2008)
63. I. Kontro et al., Effects of phosphonium-based ionic liquids on phospholipid membranes studied by small-angle X-ray scattering. Chem. Phys. Lipid. **201**, 59–66 (2016)
64. S. Mitra, S.K. Ghosh, Effect of ionic liquids on the structures of ripple phases of model cellular membranes. In *AIP Conference Proceedings*. Vol. 2265. 1. AIP Publishing (2020)
65. T. Salditt, C. Li, A. Spaar, Structure of antimicrobial peptides and lipid membranes probed by interface-sensitive X-ray scattering. Biochim. Biophys. Acta (BBA)-Biomembr. **1758**(9), 1483–1498 (2006)
66. S. Tristram-Nagle et al., Measurement of chain tilt angle in fully hydrated bilayers of gel phase lecithins. Biophys. J . **64**(4), 1097–1109 (1993)
67. S.A. Tristram-Nagle, Preparation of oriented, fully hydrated lipid samples for structure determination using X-ray scattering. Methods Membr. Lipids **400**, 63–75 (2007)
68. R. Gupta et al., Ionic liquid-induced phase-separated domains in lipid multilayers probed by x-ray scattering studies. ACS Omega **6**(7), 4977–4987 (2021)
69. S.K. Ghosh, S. Aeffner, T. Salditt, Effect of PIP2 on bilayer structure and phase behavior of DOPC: an X-ray scattering study. ChemPhysChem **12**(14), 2633–2640 (2011)
70. Y. Ma et al., Anomalous partitioning of water in coexisting liquid phases of lipid multilayers near 100% relative humidity. Phys. Chem. Chem. Phys. **18**(2), 1225–1232 (2016)
71. J.F. Nagle, S. Tristram-Nagle, Structure of lipid bilayers. Biochim. Biophys. Acta (BBA)-Rev. Biomembr. **1469**(3), 159–195 (2000)

72. T. Salditt, G. Brotons, Biomolecular and amphiphilic films probed by surface sensitive X-ray and neutron scattering. Anal. Bioanal. Chem. **379**, 960–973 (2004)
73. M. Seul, M.J. Sammon, Preparation of surfactant multilayer films on solid substrates by deposition from organic solution. Thin Solid Films **185**(2), 287–305 (1990)
74. Y. Ma et al., Cholesterol partition and condensing effect in phase-separated ternary mixture lipid multilayers. Biophys. J. **110**(6), 1355–1366 (2016)
75. M. Porras-Gómez et al., Multiscale compression-induced restructuring of stacked lipid bilayers: from buckling delamination to molecular packing. PLoS One **17**(12), e0275079 (2022)
76. L. Tayebi et al., Long-range interlayer alignment of intralayer domains in stacked lipid bilayers. Nat. Mater. **11**(12), 1074–1080 (2012)
77. J. Als-Nielsen, D. McMorrow, *Elements of Modern X-ray Physics* (Wiley, 2011)
78. J. Bahadur, A. Das, D. Sen, Evaporation-induced structural evolution of the lamellar mesophase: a time-resolved small-angle X-ray scattering study. J. Appl. Crystallogr. **52**(5), 1169–1175 (2019)
79. P. Hitaishi et al., Cholesterol-controlled interaction of ionic liquids with model cellular membranes. Langmuir **39**(27), 9396–9405 (2023)
80. P. Hitaishi, P. Mandal, S.K. Ghosh, Partitioning of a hybrid lipid in domains of saturated and unsaturated lipids in a model cellular membrane. ACS Omega **6**(50), 34546–34554 (2021)
81. S. Karmakar, V.A. Raghunathan, Cholesterol-induced modulated phase in phospholipid membranes. Phys. Rev. Lett. **91**(9), 098102 (2003)
82. M.J. Janiak, D.M. Small, G. Graham Shipley, Nature of the thermal pretransition of synthetic phospholipids: dimyristoyl-and dipalmitoyllecithin. Biochemistry **15**(21), 4575–4580 (1976)
83. L.G. Parratt, Surface studies of solids by total reflection of X-rays. Phys. Rev. **95**(2), 359 (1954)
84. E. Chason, T.M. Mayer, Thin film and surface characterization by specular X-ray reflectivity. Crit. Rev. Solid State Mater. Sci. **22**(1), 1–67 (1997)
85. K. Kjaer et al., An x-ray scattering study of lipid monolayers at the air-water interface and on solid supports. Thin Solid Films **159**(1–2), 17–28 (1988)
86. C.A. Helm et al., Phospholipid monolayer density distribution perpendicular to the water surface. A synchrotron X-ray reflectivity study. Europhys. Lett. **4**(6), 697 (1987)
87. A. Das et al., Data-reduction procedure for correction of geometric factors in the analysis of specular X-ray reflectivity of small samples. J. Appl. Crystallogr. **51**(5), 1295–1303 (2018)
88. A. Greco et al., Neural network analysis of neutron and X-ray reflectivity data: automated analysis using mlreflect, experimental errors and feature engineering. J. Appl. Crystallogr. **55**(2), 362–369 (2022)
89. A. Gibaud, G. Vignaud, S.K. Sinha, The correction of geometrical factors in the analysis of X-ray reflectivity. Acta Crystallogr. A **49**(4), 642–648 (1993)
90. M. Yasaka et al., X-ray thin-film measurement techniques. Rigaku J. **26**(2), 1–9 (2010)
91. P.S. Pershan, X-ray scattering from liquid surfaces: effect of resolution. J. Phys. Chem. B **113**(12), 3639–3646 (2009)
92. C.A. Helm et al., Phospholipid monolayers between fluid and solid states. Biophys. J . **52**(3), 381–390 (1987)
93. H. Brockman, Lipid monolayers: why use half a membrane to characterize protein-membrane interactions? Curr. Opin. Struct. Biol. **9**(4), 438–443 (1999)
94. A. Chachaj-Brekiesz et al., Electrical properties of membrane phospholipids in Langmuir monolayers. Membranes **11**(1), 53 (2021)
95. A. Korytowski et al., Impact of lipid oxidization on vertical structures and electrostatics of phospholipid monolayers revealed by combination of specular X-ray reflectivity and grazing-incidence X-ray fluorescence. J. Phys. Chem. B **119**(30), 9787–9794 (2015)
96. R.P. Giri, A. Chakrabarti, M.K. Mukhopadhyay, Cholesterol-induced structural changes in saturated phospholipid model membranes revealed through X-ray scattering technique. J. Phys. Chem. B **121**(16), 4081–4090 (2017)
97. T.R. Jensen, K. Kjaer, Structural properties and interactions of thin films at the air-liquid interface explored by synchrotron X-ray scattering. Novel Methods Study Interfacial Layers **11**, 2054 (2001)
98. K. Kjaer et al., Ordering in lipid monolayers studied by synchrotron x-ray diffraction and fluorescence microscopy. Phys. Rev. Lett. **58**(21), 2224 (1987)
99. P. Mandal et al., Self-assembly of graphene oxide nanoflakes in a lipid monolayer at the air-water interface. ACS Appl. Mater. Interfaces **13**(48), 57023–57035 (2021)
100. D.M. Kamiński et al., Effect of cholesterol and ergosterol on the antibiotic amphotericin B interactions with dipalmitoylphosphatidylcholine monolayers: X-ray reflectivity study. Biochim. Biophys. Acta (BBA)-Biomembr. **1838**(11), 2947–2953 (2014)
101. R.P. Richter, R. Bérat, A.R. Brisson, Formation of solid-supported lipid bilayers: an integrated view. Langmuir **22**(8), 3497–3505 (2006)
102. E.T. Castellana, P.S. Cremer, Solid supported lipid bilayers: from biophysical studies to sensor design. Surf. Sci. Rep. **61**(10), 429–444 (2006)
103. C.E. Miller, J. Majewski, T.L. Kuhl, Characterization of single biological membranes at the solid-liquid interface by X-ray reflectivity. Colloids Surf. A **284**, 434–439 (2006)
104. E.B. Watkins et al., Structure and thermodynamics of lipid bilayers on polyethylene glycol cushions: fact and fiction of PEG cushioned membranes. Langmuir **27**(22), 13618–13628 (2011)

105. G. Bhattacharya et al., X-ray reflectivity study of the interaction of an imidazolium-based ionic liquid with a soft supported lipid membrane. Langmuir **33**(5), 1295–1304 (2017)
106. R.P. Giri, M.K. Mukhopadhyay, Humidity-responsive polymer cushion-supported biomimetic membrane: a model system for X-ray studies. Langmuir **38**(49), 15294–15302 (2022)
107. J.K. Basu, M.K. Sanyal, Ordering and growth of Langmuir-Blodgett films: X-ray scattering studies. Phys. Rep. **363**(1), 1–84 (2002)
108. G.H. Vineyard, Grazing-incidence diffraction and the distorted-wave approximation for the study of surfaces. Phys. Rev. B **26**(8), 4146 (1982)
109. H. Dosch, Evanescent X-rays probing surface-dominated phase transitions. Int. J. Mod. Phys. B **6**(17), 2773–2808 (1992)
110. M. Neuschitzer et al., Grazing-incidence in-plane X-ray diffraction on ultra-thin organic films using standard laboratory equipment. J. Appl. Crystallogr. **45**(2), 367–370 (2012)
111. J. Pignat et al., Grazing incidence x-ray diffraction on Langmuir films: Toward atomic resolution. J. Phys. Chem. B **110**(44), 22178–22184 (2006)
112. M. Broniatowski et al., Grazing incidence diffraction and X-ray reflectivity studies of the interactions of inorganic mercury salts with membrane lipids in Langmuir monolayers at the air/water interface. J. Phys. Chem. B **114**(29), 9474–9484 (2010)
113. A.L. Patterson, The Scherrer formula for X-ray particle size determination. Phys. Rev. **56**(10), 978 (1939)
114. R. Zsigmondy, P. Scherrer, "Bestimmung der inneren Struktur und der Größe von Kolloidteilchen mittels Röntgenstrahlen". Kolloidchemie Ein Lehrbuch, 387–409 (1912)
115. X. Wang et al., Structural changes of phospholipid monolayers caused by coupling of human serum albumin: a GIXD study at the air/water interface. J. Phys. Chem. B **108**(37), 14171–14177 (2004)
116. F. Neville et al., Protegrin interaction with lipid monolayers: grazing incidence X-ray diffraction and X-ray reflectivity study. Soft Matter **4**(8), 1665–1674 (2008)
117. S. Behyan et al., Nanoparticle-induced structural changes in lung surfactant membranes: an X-ray scattering study. Environ. Sci. Nano **5**(5), 1218–1230 (2018)
118. N.N. Casillas-Ituarte et al., Na+ and Ca2+ effect on the hydration and orientation of the phosphate group of DPPC at air- water and air- hydrated silica interfaces. J. Phys. Chem. B **114**(29), 9485–9495 (2010)
119. P. Maity et al., Binding of monovalent alkali metal ions with negatively charged phospholipid membranes. Biochim. Biophys. Acta (BBA)-Rev. Biomembr. **1858**(4), 706–714 (2016)
120. P. Maity et al., Effect of zwitterionic phospholipid on the interaction of cationic membranes with monovalent sodium salts. Langmuir **34**(33), 9810–9817 (2018)
121. P.K. Bera et al., Grazing incidence X-ray diffraction studies of lipid-peptide mixed monolayers during shear flow. ACS Omega **5**(24), 14555–14563 (2020)
122. E.B. Watkins et al., Structure and orientational texture of self-organizing lipid bilayers. Phys. Rev. Lett. **102**(23), 238101 (2009)
123. E.B. Watkins et al., Equilibrium or quenched: fundamental differences between lipid monolayers, supported bilayers, and membranes. ACS Nano **8**(4), 3181–3191 (2014)
124. M. Dhanasekaran, M. Jaganathan, A. Dhathathreyan, Colloids versus solution state adsorption of proteins: Interaction of Myoglobin with supported lipid bilayers. Int. J. Biol. Macromol. **114**, 434–440 (2018)
125. J. Pusterla et al., Characterization of lipid bilayers adsorbed to functionalized air/water interfaces. Nanoscale **14**(40), 15048–15059 (2022)
126. V. Cherezov, K.M. Riedl, M. Caffrey, Too hot to handle? Synchrotron X-ray damage of lipid membranes and mesophases. J. Synchrotron Radiat. **9**(6), 333–341 (2002)
127. S. Qian, V.K. Sharma, L.A. Clifton, Understanding the structure and dynamics of complex biomembrane interactions by neutron scattering techniques. Langmuir **36**(50), 15189–15211 (2020)